

1 **Temporal and Spatial Variability of Ammonia in Urban and Agricultural Regions**
2 **of Northern Colorado, United States**

3

4 Yi Li^{1,5}, Tammy M. Thompson², Martin Van Damme³, Xi Chen¹, Katherine B. Benedict¹,
5 Yixing Shao¹, Derek Day², Alexandra Boris¹, Amy P. Sullivan¹, Jay Ham⁴, Simon
6 Whitburn³, Lieven Clarisse³, Pierre-François Coheur³ and Jeffrey L. Collett, Jr.^{1*}

7

8 ¹Department of Atmospheric Science, Colorado State University, Fort Collins, Colorado,
9 USA.

10 ²Cooperative Institute for Research in the Atmosphere/NPS, Colorado State University,
11 Fort Collins, Colorado, USA.

12 ³Atmospheric Spectroscopy, Université Libre de Bruxelles (ULB), Brussels, Belgium

13 ⁴Department of Soil & Crop Sciences, Colorado State University, Fort Collins, Colorado,
14 USA.

⁵ now, Arizona Department of Environmental Quality, Air Quality Division, Phoenix, AZ,
 USA

15

16

17 **Abstract**

18 Concentrated agricultural activities and animal feeding operations in the northeastern
19 plains of Colorado represent an important source of atmospheric ammonia (NH₃). The NH₃

*Corresponding author: Jeffrey L. Collett Jr., Department of Atmospheric Science, Colorado State University, Fort Collins, Colorado, 80523, USA (collett@atmos.colostate.edu)

from these sources contributes to regional fine particle formation and to nitrogen deposition to sensitive ecosystems in Rocky Mountain National Park (RMNP), located ~80 km to the west. In order to better understand temporal and spatial differences in NH_3 concentrations in this source region, weekly concentrations of NH_3 were measured at 14 locations during the summers of 2010 to 2015 using Radiello passive NH_3 samplers. Weekly (biweekly in 2015) average NH_3 concentrations ranged from $2.66 \mu\text{g}/\text{m}^3$ to $42.7 \mu\text{g}/\text{m}^3$, with the highest concentrations near large concentrated animal feeding operations (CAFOs). The annual summertime mean NH_3 concentrations were stable in this region from 2010 to 2015, providing a baseline against which concentration changes associated with future changes in regional NH_3 emissions can be assessed. Vertical profiles of NH_3 were also measured on the 300 m Boulder Atmospheric Observatory (BAO) tower throughout 2012. The highest NH_3 concentration along the vertical profile was always observed at the 10 m height (annual average concentration of $4.63 \mu\text{g}/\text{m}^3$), decreasing toward the surface ($4.35 \mu\text{g}/\text{m}^3$) and toward higher altitudes ($1.93 \mu\text{g}/\text{m}^3$). The NH_3 spatial distributions measured using the passive samplers are compared with NH_3 columns retrieved by the Infrared Atmospheric Sounding Interferometer (IASI) satellite and concentrations simulated by the Comprehensive Air quality Model with extensions (CAMx). The satellite comparison adds to a growing body of evidence that IASI column retrievals of NH_3 provide very useful insight into regional variability in atmospheric NH_3 , in this case even in a region with strong local sources and sharp spatial gradients. The CAMx comparison indicates that the model does a reasonable job simulating NH_3 concentrations near sources but tends to underpredict concentrations at locations farther downwind. Excess NH_3 deposition by the model is hypothesized as a possible explanation for this trend.

43

44 **1. Introduction**

45 As the most abundant basic gas in the atmosphere, ammonia (NH_3) can neutralize ambient
46 acidic species, such as sulfuric acid (H_2SO_4) and nitric acid (HNO_3), to form ammonium
47 salts, which are the dominant inorganic compounds in ambient $\text{PM}_{2.5}$ (particulate matter
48 with aerodynamic diameter less than $2.5\ \mu\text{m}$). $\text{PM}_{2.5}$ has been linked to adverse effects on
49 human health (Davidson et al., 2005; Schwartz and Neas, 2000; Lelieveld et al., 2015) and
50 regional visibility reduction (Park et al., 2006) and also impacts climate via direct and
51 indirect changes in radiative forcing (Langridge et al., 2012; Parry et al., 2007). While the
52 atmospheric lifetime of NH_3 is short (on the order of hours to days due to rapid dry
53 deposition and particle-forming chemical reactions), ammonium (NH_4^+) salts are mainly
54 found in submicron aerosol particles and have longer atmospheric lifetimes (on the order
55 of several days) so that they can be transported to remote areas away from NH_3 sources
56 (Aneja et al., 2001; Fowler et al., 1998; Ianniello et al., 2011). Dry and wet deposition of
57 NH_3 and NH_4^+ also play an important role in the adverse effects of increased nitrogen
58 deposition to sensitive ecosystems (Asman et al., 1998; Beem et al., 2010; Benedict et al.,
59 2013b; Horii et al., 2006; Paulot et al., 2013). Li et al. (2016) analyzed wet and dry
60 deposition of reactive nitrogen across the U.S. and found that reduced nitrogen, derived
61 from NH_3 emissions, now constitutes the majority of inorganic nitrogen deposition in most
62 regions.

63

64 It is widely believed that agriculture represents the largest source of atmospheric NH_3
65 globally, but at smaller spatial scales the influence of agriculture varies greatly. Sutton et

al. (2013) estimated that 57% of global atmospheric NH_3 is emitted from livestock and crops, while the U.S. Environmental Protection Agency (EPA) attributed over 82% of NH_3 emissions in the U.S. to the agricultural sector in the 2014 National Emissions Inventory (NEI, <https://www.epa.gov/air-emissions-inventories/2014-national-emissions-inventory-nei-data>). Hertel et al. (2006) also found that deposition of atmospheric NH_3 near an intensive agricultural area would dominate the overall load of reactive nitrogen (N) from the atmosphere. Agricultural NH_3 emissions have become one of the most prominent air pollution problems in recent years and have given rise to growing concerns (Aneja et al., 2006; Pan et al., 2012; Bauer et al., 2016). Within the U.S., efforts to routinely monitor NH_3 concentrations have been growing via the Ammonia Monitoring Network (AMON; <http://nadp.sws.uiuc.edu/AMoN/sites/data/>). NH_3 can now be considered as a precursor to $\text{PM}_{2.5}$ in the state implementation planning process for meeting the national ambient air quality standards, and voluntary reductions in agricultural NH_3 emissions have been prioritized as part of efforts to reduce reactive nitrogen deposition in Rocky Mountain National Park (<http://www.rmwarningsystem.com/ReducingAmmoniaEmissions.aspx>). Besides the dominant contributions from agricultural sources, ambient NH_3 also originates from other sources such as vehicles with three-way catalysts (Shelef and Gandhi, 1974; Chang et al., 2016). Biomass burning (such as wildfires) is another important source of NH_3 (Benedict et al., 2017): in the 2014 U.S. NEI, wildfires make up nearly 4.3% of national NH_3 emissions.

The northeastern plains of Colorado include the Denver-Fort Collins urban corridor along the Front Range and a large agricultural region reaching eastward toward the border with

Nebraska. This area has been recognized as an important NH_3 emission source region, and the largest reduced nitrogen source near Rocky Mountain National Park (RMNP) (Benedict et al., 2013c; Ellis et al., 2013). According to the 2002 Front Range NH_3 emission inventory, NH_3 emissions from the Front Range were 10288 tons/year from livestock and 5183 tons/year from fertilizer application, which accounted for 30% and 27% of Colorado's NH_3 emissions, respectively (according to RMNP Initiative – Nitrogen Deposition Reduction Contingency Plan, 2010). The Rocky Mountain Atmospheric Nitrogen and Sulfur (RoMANS) studies (<https://www.nature.nps.gov/air/studies/romans.cfm>, Beem et al., 2010;Benedict et al., 2013c;Malm et al., 2013;Thompson et al., 2015;Malm et al., 2016), conducted in 2006 and 2009, showed that together NH_3 and NH_4^+ contributed approximately 50% of the total reactive nitrogen deposition (both wet and dry) in RMNP, with the remainder coming from dry and wet deposition of nitrate and organic nitrogen (Benedict et al., 2013a). The highest concentrations of particulate NH_4^+ measured during RoMANS were associated with upslope transport from the east side of RMNP, indicating major sources of NH_3 to RMNP are located in the northeastern plains of Colorado (Benedict et al., 2013c;Beem et al., 2010;Eilerman et al., 2016). In 2010, an effort was initiated to map the NH_3 concentrations in Northern Colorado and significant NH_3 spatial differences were found, with averages ranging from $3.43 \mu\text{g}/\text{m}^3$ at rural grasslands to $10.7 \mu\text{g}/\text{m}^3$ at suburban-urban sites and $31.5 \mu\text{g}/\text{m}^3$ near an area of concentrated animal feeding operations (CAFOs) (Day et al., 2012).

Due to the short atmospheric lifetime and high dry deposition velocity of NH_3 , there are many factors, such as the height of the boundary layer, surface properties, location of

sources, local advection and the vertical mixing rate, that influence spatial (horizontal and vertical) distributions of NH_3 concentrations. This complex dependence of NH_3 concentrations on atmospheric conditions and deposition variability results in great uncertainties of NH_3 concentrations in global and regional atmospheric chemistry models (Sutton et al., 2008;Zhu et al., 2013). Several model performance evaluations (MPEs) have found model predictions of NH_3 concentrations in the western U.S. to be low (Rodriguez et al., 2011;Thompson et al., 2015;Battye et al., 2016). Rodriguez et al. (2011) and (Thompson et al., 2015) utilized the Comprehensive Air quality Model with extensions (CAMx); Battye et al. (2016), meanwhile, ran a different photochemical model (CMAQ), and utilized emissions inventories generated with less focus on the precise spatial positioning of agricultural sector emissions in the Inter-Mountain West. Evaluation of NH_3 concentration prediction performance in larger scale models has suggested that uncertainty in emissions inventories is a cause of NH_3 concentration under-estimation in the west (Zhu et al., 2013;Heald et al., 2012). Van Damme et al. (2015) used measured NH_3 data from the U.S., China, Africa, and Europe (ground-based and airborne observations) and compared these data with IASI- NH_3 columns. During the DISCOVER-AQ campaign, Sun et al. (2015) also compared *in situ* observations (airborne and vehicle-based) with Tropospheric Emission Spectrometer (TES) NH_3 columns. Both comparisons demonstrated fair agreement between *in situ* measurements and satellite total columns, indicating that NH_3 data from *in situ* measurements and satellite retrievals are reliable. The discrepancy between model predictions and observations of NH_3 concentrations suggests that variability in the spatial and/or temporal distribution of NH_3 is not captured by current emissions inventories or model inputs, and additional understanding of atmospheric NH_3

distributions, for example, with height above ground level, is needed. Vertical NH₃ profiles have previously been reported from airborne studies such as CalNex (Nowak et al., 2012;Schiferl et al., 2014), the DISCOVER-AQ campaign (Sun et al., 2015;Müller et al., 2014), and from measurements made at the Canadian oil sands (Shephard et al., 2015). These studies have found strong variation of NH₃ concentration above ground, but do not provide a sufficient basis to characterize the general vertical distribution of NH₃ with limited sampling periods.

The primary goal of this study is to investigate the spatial and temporal variability of NH₃ concentrations in the northeastern plains of Colorado. This effort builds upon the earlier efforts of Benedict et al. (2013c), Day et al. (2012), and Battye et al. (2016) to look at patterns of spatial variability across several years with different meteorology and source strength (e.g., years with and without active fire seasons) and to identify any multi-year trends in regional NH₃ concentrations. Year-round measurements of the vertical profile of NH₃ measured using a 300 m tower near Erie, Colorado will also provide new insight into the vertical profile of NH₃ concentrations in the lower atmosphere and its change with season. The *in situ* surface and tower measurements will also be compared to NH₃ remote sensing measurements from the Infrared Atmospheric Sounding Interferometer (IASI) satellite (Whitburn et al., 2016;Van Damme et al., 2015) and predictions from CAMx to provide insight into the regional performance of each. Many recent and past MPEs have utilized special studies, such as the one presented in this paper, to evaluate photochemical model performance with respect to NH₃. Overall, our results are useful for determining important sources contributing to regional nitrogen deposition, validating emission

inventories and concentration predictions for atmospheric chemistry models, and setting a baseline against which concentration changes resulting from future emission changes can be assessed.

2. Methodology

2.1 Site descriptions

The northeastern plains of Colorado are an intensive agricultural area with many CAFOs, including beef cattle feedlots and dairy operations. The densely populated Front Range urban corridor is located just west of this area, and just east of the Rocky Mountains. In order to gain information about spatial variability of northeast Colorado NH_3 concentrations, fourteen monitoring sites were selected in the region according to land use categories and distance from known, major NH_3 sources (Table 1). Five suburban monitoring sites located in the Front Range urban corridor are representative of areas with little local agricultural influence, especially from animal feeding operations: Louisville (LE), western Fort Collins (FC_W), Loveland (LD), Loveland Golf Course (LGC) and the Boulder Atmospheric Observatory (BAO) tower. Three rural sites (Nunn, NN; Briggsdale, BE; and Ranch, RH), located close to the northern boundary of Colorado with Wyoming, are grassland sites with minimal local agricultural influence. Three suburban sites (eastern Fort Collins, FC_E; Severance, SE; and Greeley, GY) as well as three rural sites (Ault, AT; Kersey, KY; and Brush, BH) represent areas close to and likely significantly influenced by agricultural activities, including animal feeding operations. For example, the KY site is located approximately 0.4 km from a large beef cattle feedlot (about 100,000 cattle capacity).

181

182 The BAO tower is a 300 m meteorological tower situated in the southern part of the
183 sampling area (40.050N, 105.004W). It has been owned and operated by the National
184 Oceanic and Atmospheric Administration (NOAA) for more than 25 years
185 (<http://www.esrl.noaa.gov/psd/technology/bao/>). The tower is surrounded by natural grass
186 and wheat fields, and is approximately 400 m west of Interstate 25 and 30 km north of
187 downtown Denver.

188

189 **2.2 Sample collection and validation**

190 In order to obtain spatial and vertical distributions of NH_3 concentrations, two sampling
191 campaigns were carried out in the northeastern plains of Colorado using Radiello passive
192 NH_3 samplers and URG (University Research Glassware, Inc.) denuder/filter-pack systems.
193 The Radiello passive NH_3 sampler consists of a cartridge adsorbent (part number:
194 RAD168), a blue microporous cylindrical diffusive body (part number: RAD1201) and a
195 vertical adapter (part number: RAD 122). All Radiello sampler components were obtained
196 from Sigma Aldrich (<http://www.sigmaaldrich.com>). Measurements of the spatial NH_3
197 distribution were conducted each summer from 2010 to 2015. During the first summer
198 (2010), measurements were made at nine sites; in 2011, the Ranch (RH) site was removed
199 and the LE and NN sites were added; in 2012, the LE site was removed; two sites, FC_E
200 and SE, were added in 2013. The two site removals in 2013 (RH and LE) and FC_E
201 removal in 2015 were both due to property access issues. In a second campaign,
202 measurements of vertical NH_3 concentration profiles were conducted at the BAO tower
203 from December 2011 to January 2013.

204

205 **2.2.1 Passive sampler**

206 Passive ammonia samplers have been used in several previous studies because of their
207 reliability, low labor intensity, simplicity and lack of power requirement (Cisneros et al.,
208 2010;Day et al., 2012;Meng et al., 2011;Reche et al., 2012;Puchalski et al., 2011). During
209 sample collection, the sampler was protected from precipitation and direct sunlight by an
210 inverted plastic bucket. Ambient NH_3 diffuses through a microporous diffusive body
211 surface and is captured as NH_4^+ by a cartridge impregnated with phosphoric acid (H_3PO_4).
212 A weekly sampling campaign period was implemented in each summer during the study:
213 May 20th to September 2nd 2010, June 2nd to August 31st 2011, June 21st to August 29th
214 2012, May 30th to August 29th 2013 and May 29th to August 28th 2014. Bi-weekly samples
215 were collected from May 26th to September 1st 2015. At the BAO tower, NH_3 was sampled
216 at nine heights: 1 m, 10 m, 22 m, 50 m, 100 m, 150 m, 200 m, 250 m, and 300 m. Vertical
217 profiles were measured across two-week sampling periods from December 13th 2011 to
218 January 9th 2013, except when weekly measurements were conducted from June 19th to
219 August 30th 2012 when higher concentrations were anticipated. Passive samplers were
220 prepared in an NH_3 -free laminar flow hood (Enviroco Corporation) and sealed for transport
221 to the field. More detailed information regarding sampler preparation can be obtained in
222 Day et al. (2012).

223

224 The ambient NH_3 concentration was calculated based on the characteristics of the passive
225 sampler and the diffusivity of NH_3 in the atmosphere (D_{NH_3}), which is a function of local
226 temperature (T) and ambient pressure (P), and can be expressed using Eq. 1:

$$D_{NH_3}(T, P) = D_{0,1} \times \left(\frac{P_0}{P}\right) \times \left(\frac{T}{T_0}\right)^{1.81} \quad (\text{Eq. 1})$$

where $D_{0,1} = 0.1978 \text{ cm}^2\text{s}^{-1}$ at $T_0 = 273 \text{ K}$ (0°C) and $P_0 = 1 \text{ atm}$ (Massman, 1998). Then, the diffusional flow rate through the NH_3 passive sampler (Q_{NH_3}) is given by Eq. 2:

$$Q_{NH_3} = D_{NH_3}(T, P) \times \frac{A}{\Delta X} \quad (\text{Eq. 2})$$

where A is the passive sampler effective cross-sectional area and ΔX is the passive sampler diffusion distance. For the Radiello NH_3 passive sampler, $A/\Delta X$ represents the geometric constant for radial flow and has been reported to be 14.2 cm , based on actual physical measurements (Day et al., 2012; Puchalski et al., 2011), which differs from the manufacturer's description (http://www.radiello.com/english/nh3_en.htm). Each diffusional flow rate (Q_{NH_3}) was calculated for the averaged T and P for each interval sampling period. Finally, the NH_3 concentration in the air (C_{NH_3}) is calculated from the diffusional flow rate (Q_{NH_3}), the duration of sampling time (t) and the mass of NH_3 collected on the cartridge (m_{NH_3}) as shown in Eq. 3:

$$C_{NH_3} = \frac{m_{NH_3}}{t \times Q_{NH_3}} \quad (\text{Eq. 3})$$

For the northeastern plains network, hourly temperature data were obtained from nearby CoAGMET weather stations (<http://www.coagmet.com/>) (Table S1). The distance between the NH_3 measurement sites and the nearby meteorological stations referenced in the paper were from 0.1 km (KSY01 to KY) to 68.1 km (BRG01 to BH), with an average value of 16.5 km . The average meteorological record was fairly consistent from year-to-year. The ambient pressure was calculated based on the elevation of each site. At the BAO tower, temperature and relative humidity were measured by battery-powered sensors (EBI20-TH1, EBRO Inc. Ingolstadt, Germany; <http://shop.ebro.com/chemistry/ebi-20-th.html>) co-located with the NH_3 passive samplers at each sampling height.

250

251 **2.2.2 URG denuder/filter-pack sampler**

252 During the same sampling periods as the NH_3 passive samplers, URG denuder/filter-pack
253 sampling systems were also installed during select campaign years at the FC_W, GY, and
254 BAO tower sites to measure the concentrations of gaseous NH_3 and HNO_3 , as well as fine
255 particulate inorganic ions. Air was drawn first through a Teflon-coated $\text{PM}_{2.5}$ cyclone
256 ($D_{50}=2.5\ \mu\text{m}$) at the inlet, followed by two annular denuders connected in series. The first
257 denuder was coated with sodium carbonate (Na_2CO_3) solution (10 g of Na_2CO_3 and 10 g
258 of glycerol dissolved in 500 ml of 18.2 M Ω -cm deionized water and 500 ml methanol) to
259 collect gaseous HNO_3 and sulfur dioxide (SO_2). The second denuder was coated with a
260 phosphorous acid (H_3PO_3) solution (10 g of H_3PO_3 dissolved in 100 ml of deionized water
261 and 900 ml methanol) to collect gaseous NH_3 in the atmosphere. The air was then drawn
262 through a filter pack containing a 47 mm nylon filter (Nylasorb, pore size 1 μm , Pall
263 Corporation) to collect fine particles, followed by a backup H_3PO_3 -coated denuder to
264 capture any NH_3 re-volatilized from NH_4^+ salt particles collected on the nylon filter. The
265 URG samplers were changed at the same time as the passive samplers during each site visit.
266 The air flow rate was controlled by a URG mass flow-controlled pump; the total flow rate
267 through the system was nominally 3 L/min at FC_W, GY, and BAO. The URG sampling
268 system has been used widely in previous studies because of its validated performance in
269 sampling gases and particles (Bari et al., 2003;Beem et al., 2010;Benedict et al., 2013b;Lee
270 et al., 2008;Li et al., 2014;Lin et al., 2006) and was used as a reference method for
271 evaluating the performance of the NH_3 passive samplers.

272

2.2.3 Sample analysis and evaluation

Passive samplers and URG denuders were extracted on arrival in the lab at Colorado State University (CSU). The URG denuders were extracted with 10 ml deionized water; the Nylon filters and passive sampler cartridges were ultrasonically extracted for 55 minutes in 6 ml and 10 ml deionized water, respectively. Passive sampler and H_3PO_3 -coated-denuder extracts were analyzed by ion chromatography for NH_4^+ , Na_2CO_3 -coated denuder extracts were analyzed for NO_3^- and SO_4^{2-} , and Nylon filter extracts were analyzed for cations (Na^+ , NH_4^+ , K^+ , Mg^{2+} and Ca^{2+}) and anions (Cl^- , NO_3^- , SO_4^{2-}). Cations in the samples were separated with a 20 mM methanesulfonic acid eluent (0.5 ml/min) on a Dionex CS12A ion exchange chromatography column configured with a CSRS ULTRA II suppressor and detected using a Dionex conductivity detector. Anions in the samples were separated with an 8 mM carbonate/1mM bicarbonate eluent (1 ml/min) on a Dionex AS14A column followed by an ASRS ULTRA II suppressor and detected using a Dionex conductivity detector (Li et al., 2014).

Replicate Radiello passive samples were collected at FC_W (2011, weekly), BH (2012, 2013 and 2014, weekly), GY (2014, weekly and 2015, bi-weekly), KY (2014, weekly) and three different heights (1 m, 100 m and 300 m) of the BAO tower (biweekly; weekly in summer) during the campaign to evaluate the performance of NH_3 passive samplers under different NH_3 concentrations and sampling periods. Comparison of replicate samples yielded good precision (see Fig. S1) with a pooled relative standard deviation of 8.9% ($n=288$). The weekly and biweekly NH_3 concentrations collected by passive samplers were also in good agreement with measurements by co-located URG denuder samplers for the

same sampling durations (a linear least-squares regression fit yielded a correlation coefficient (R^2) between the two methods of 0.92 with a slope of 0.98 and a small positive intercept ($0.25 \mu\text{g}/\text{m}^3$) with $n=136$ collocated measurements; Fig. S2). These findings are consistent with previous studies (Benedict et al., 2013b; Day et al., 2012; Puchalski et al., 2011). Field and laboratory blanks were collected throughout the research campaign and used to blank correct sample results and determine the minimum detection limits (MDL). From the field blanks, the MDL was calculated to be $0.27 \mu\text{g}/\text{m}^3$ for a one-week Radiello passive NH_3 sample.

2.3 Satellite retrievals of ammonia

The Infrared Atmospheric Sounding Interferometer (IASI) is a passive infrared Fourier transform spectrometer onboard the MetOp platforms, operating in nadir (Clerbaux et al., 2009). IASI provides a quasi-global coverage twice a day with overpass times at around 9:30 am and 9:30 pm (when crossing the equator) at a relatively small pixel size (circle with 12 km diameter at nadir, distorted to ellipse-shaped pixels off-nadir). The combination of low instrumental noise ($\sim 0.2 \text{ K}$ at 950 cm^{-1} and 280 K), a medium spectral resolution (0.5 cm^{-1} apodized) and a continuous spectral coverage between 645 and 2760 cm^{-1} makes IASI a suitable instrument to measure various constituents of the atmosphere (Clarisse et al., 2011).

The IASI- NH_3 data set used in this work is based on a recently developed retrieval scheme presented in detail in Whitburn et al. (2016). The first step of the retrieval scheme is to calculate a so-called Hyperspectral Range Index (HRI) for each IASI spectrum, which is

representative of the amount of NH₃. This HRI is subsequently converted into NH₃ total columns using a neural network (NN) approach. It is an extension of the HRI method presented in Van Damme et al. (2014a) who used two-dimensional look-up tables (LUTs) for the radiance-concentration conversion. The new NN-based method inherits the advantages of the LUT-based HRI method whilst providing several significant improvements such as: (1) better sensitivity at low concentrations due to the large variation in temperature, pressure and humidity vertical profiles in the retrieval; (2) a reduction of the reported positive bias of LUT retrieval at low concentrations; (3) the possible consideration of NH₃ vertical profile information from third party sources; and (4) a full uncertainty characterization of the retrieved column variables (Whitburn et al., 2016). The IASI sensitivity to NH₃ is dependent on the thermal contrast (TC), defined as the temperature difference between the surface and the air at the surface. With a TC of 5, 10 and 15 K, the detection limit at one sigma is respectively 6.3×10^{15} , 3.3×10^{15} and 2×10^{15} molec/cm². In Northern Colorado, the TC during the summer period for the morning overpass of IASI is around 10 K.

2.4 Ammonia modeling

Chemical transport models are valuable tools for evaluating how various processes influence ambient air quality and pollutant deposition. They can be especially helpful in designing effective source control strategies for air quality improvement. Unfortunately, current models frequently have difficulties accurately simulating spatial concentrations of NH₃ (Battye et al., 2016; Adelman et al., 2015). In addition to the typical model difficulties in accurately simulating transport, NH₃ emissions are not well constrained (Zhu et al., 2013)

and the parameterization of NH₃ deposition is challenging (Bash et al., 2013;Pleim et al., 2013). In order to examine some of these issues, NH₃ measurements from this study are compared to modeled concentrations from the Comprehensive Air Quality Model with extensions (CAMx, http://www.camx.com/files/camxusersguide_v6-20.pdf). CAMx, a photochemical model that simulates the emissions, transport, chemistry and removal of chemical species in the atmosphere, is one of U.S. EPA's recommended regional chemical transport models and is frequently used for air quality analysis (EPA, 2007, 2011). The 2011 modelled period presented here (version base_2011a), including inputs representing emissions and meteorology, was developed for the Western Air Quality Data Warehouse (IWDW-WAQS, 2015); details on modeling protocol and model performance are available on the IWDW website (<http://views.cira.colostate.edu/tsdw/>).

3 Results and discussion

3.1 Spatial distributions of ammonia

Large spatial differences in NH₃ concentrations were found in the northeastern plains of Colorado with mean NH₃ concentrations ranging from 2.66 µg/m³ to 42.7 µg/m³ as illustrated in Fig. 1. Also included in Fig. 1 are, for qualitative comparisons, estimated NH₃ emissions from major feedlots in northeastern Colorado. The feedlots were classified into categories based on the type of animals raised (data were provided by the Colorado Department of Public Health and Environment) and NH₃ emissions were calculated following Eq. 4:

$$\text{NH}_3 \text{ Emission} = \sum (\text{Population} \times \text{Emission Factor}) \quad (\text{Eq. 4})$$

where the NH_3 emissions are the total NH_3 emitted from each feedlot in tons per year (converted from kg to tons for Fig. 1), population is the animal population in each feedlot and the emission factor was specified for each kind of animal: 44.3, 38.1, 3.37, 0.27, 6.50 and 12.2 kg NH_3 /head/year, for beef cattle, dairy cows, sheep, poultry, swine and horses, respectively (USEPA, 2004; Todd et al., 2013). 73% of the total regional feedlot emissions are contributed by beef feedlots. Many large sources are located within several tens of km to the south, east, and north of Greeley. Other large sources are located further east along the South Platte River with some smaller sources (mostly dairies) located further west in the sampling region, closer to the urban corridor. The lowest average ambient NH_3 concentrations from 2010 to 2015 in the sampling network were found at remote grassland sites such as NN and BE: $2.66 \mu\text{g}/\text{m}^3$ and $3.07 \mu\text{g}/\text{m}^3$, respectively (Table 2). Concentrations of NH_3 at suburban sites were somewhat higher than at these remote, rural sites, indicating possible impacts of human activities such as emissions from vehicles equipped with three-way catalytic converters, local waste treatment, and fertilization of yards and parks on local NH_3 concentrations. The measured weekly average NH_3 concentration at the Loveland golf course (GC) site was $5.14 \mu\text{g}/\text{m}^3$ with a range of $1.81 \mu\text{g}/\text{m}^3$ to $7.87 \mu\text{g}/\text{m}^3$, showing only slightly elevated values compared to NH_3 concentrations at other nearby suburban sites (FC_W and LD) suggesting that golf course fertilization at this location is probably not a major, regional NH_3 source. However, the NH_3 concentrations at the GC were modestly higher (17% on average) than NH_3 sampled at the LD site during each summer measurement campaign (Table 2), suggesting that the contributions from fertilization of the golf lawn cannot be neglected. The highest ambient NH_3 concentrations were consistently observed at sites near extensive animal feeding

operations. Compared to the remote sites (NN and BE), an approximately two- to five-fold increase in NH_3 concentrations was observed at rural sites BH and AT (6.17 and 13.8 $\mu\text{g}/\text{m}^3$), which were under the influence of nearby animal feeding operation emissions. A 15-fold increase in mean NH_3 concentrations was observed from the grassland NN and BE sites (2.66 and 3.07 $\mu\text{g}/\text{m}^3$) to KY (42.73 $\mu\text{g}/\text{m}^3$), 0.4 km from a feedlot with almost 100,000 cattle.

The inter-annual variation of average summertime NH_3 concentrations sampled at each site spanning several years exhibited a statistically significant ($p < 0.1$) trend (Fig. 2) at three sites; six sites showed no significant trend. Both the GY and KY sites show increasing trends, while BH exhibits a decreasing trend. Trend analysis was conducted using Theil regression (Theil, 1992) and the Mann-Kendall test (Gilbert, 1987; Marchetto et al., 2013). We define an increasing (decreasing) trend as a positive (negative) slope of the Theil regression, while the statistical significance of a trend was determined by the Mann-Kendall test (p -value). A 90th percentile significance level ($p < 0.10$) was assumed as in a previous study (Hand et al., 2012). The power of these analyses are limited by the relatively small number of measurement years to date; additional power for assessing interannual trends will become available as the measurement record lengthens. Data from the Colorado Agricultural Statistics Report (2014, http://www.nass.usda.gov/Statistics_by_State/Colorado/Publications/Annual_Statistical_Bulletin/Bulletin2015.pdf) indicate that Weld, Larimer, and Morgan counties (three major counties located in the northeastern plains of Colorado) did not show significant growth in livestock numbers between 2009 and 2014. The total annual numbers of beef cattle, milk

cows, cattle and calves in these counties were 986, 974, 996, 1065, 955 and 936 thousand head, respectively, in the six years from 2009 to 2014.

A number of best management practices (BMPs) (<http://www.rmwarningsystem.com/ReducingAmmoniaEmissions.aspx>) are under evaluation to help agricultural producers in the region to lower NH_3 emissions as part of efforts to reduce reactive nitrogen deposition in Rocky Mountain National Park. The baseline regional concentration information gathered here will be critical in helping to evaluate the success of future efforts to reduce NH_3 emissions.

Weekly average atmospheric NH_3 concentrations at each observation site are plotted for summers 2010-2015 in Fig. 3. These observations again show the general similarity, at a given location, of summertime concentrations across several years. Some variation from week to week is expected due to differences in meteorology. Emissions, for example, are dependent on the temperature, dispersion is influenced by turbulence and mixing layer depth, and removal is influenced by precipitation and turbulence. One clear outlier period is the elevated NH_3 concentrations observed at FC_W at the beginning of summer 2012 (Fig. 3c). The maximum weekly average NH_3 concentration at this site ($8.55 \mu\text{g}/\text{m}^3$) was measured during June 21-28, 2012 and was more than two times the average NH_3 concentration in 2010 ($4.13 \mu\text{g}/\text{m}^3$) and 2011 ($3.76 \mu\text{g}/\text{m}^3$) (see Table 2). This is supported by the satellite observation reported by IASI (see Section 3.3 and Fig. 7). During this elevated concentration period, the High Park Fire, one of the largest fires recorded in Colorado history at 353 km^2 burned, was burning in the mountains west of Fort Collins

and the city was frequently impacted by smoke. The fire was first spotted on June 9, 2012 and declared 100% contained on June 30, 2012 (http://en.wikipedia.org/wiki/High_Park_fire). During the wildfire period, on-line instruments (Picarro NH₃ analyzer and Teledyne CO analyzer) were also set up to measure CO and NH₃ concentrations near the FC_W site. A significant correlation between CO and NH₃ was found during the wildfire (Prenni et al., 2012; Benedict et al., 2017). The FC_W site was the closest site to the High Park Fire and normally has relatively low ambient NH₃ concentration. The NH₃ emitted from the High Park Fire may also have reached other, more distant sites downwind; however, enhanced NH₃ concentrations at these sites from other nearby sources and the greater dilution of the smoke plume as it travels further downwind make it difficult to identify any impacts of the wildfire at these locations. Elevated NH₃ concentrations in the High Park Fire plume are evidence of the importance of wild and prescribed burning as a source of atmospheric NH₃, reinforcing similar findings from previous studies (Coheur et al., 2009; Prenni et al., 2014; Sutton et al., 2000; Whitburn et al., 2015; Luo et al., 2015).

3.2 Vertical distribution of ammonia

While surface measurements of NH₃ concentrations remain uncommon, measurements of vertical profiles of NH₃ concentrations above the surface are more rare, with the exception of a small number of aircraft measurements over limited time frames as mentioned in the introduction. Time series of vertical profiles of ambient NH₃ concentrations measured at the BAO tower across the full year of 2012 are shown in Fig. 4. During most sampling periods, the NH₃ concentration exhibited a maximum at 10 m decreasing both toward the

lowest (1 m) measurement point and with height above 10 m. The minimum concentration was observed at the highest measurement point at the top (300 m) of the BAO tower. While the major sources of NH_3 are surface emissions, it is not surprising to see a gradient of decreasing concentration near the surface at this location where local emissions are expected to be small and the net local flux represents surface deposition (Pul et al., 2009). The long time duration of the integration period (1-2 weeks) in this study precludes a meaningful determination of surface removal rates based on the observed concentration gradient.

Seasonal variations in the vertical profile of NH_3 are depicted in Fig. 5 with March, April and May defined as spring; June, July and August as summer; September, October and November as fall; and December, January and February as winter. Vertical concentration differences were greatest in winter (from an average concentration greater than $4 \mu\text{g}/\text{m}^3$ near the surface to approximately $1 \mu\text{g}/\text{m}^3$ at 300 m, representing a decrease of approximately 75%) followed by fall ($1.9 \mu\text{g}/\text{m}^3$ near the surface and $4.5 \mu\text{g}/\text{m}^3$ at 300 m). Low level temperature inversions which trap emissions closer to the surface are common in both seasons (fall and winter). The highest concentrations across the profile were observed in summer, when volatility of NH_3 increases due to higher temperatures and vertical mixing is enhanced. The concentration decrease from the surface to 300 m averaged only 44% in summer. Increased NH_3 concentrations in summer also may reflect a shift in thermodynamic equilibrium of particulate NH_4NO_3 toward its gas phase precursors NH_3 and HNO_3 . Previous studies have reported increased NH_3 concentrations in summer and/or reduced concentrations in winter due to the seasonal changes of NH_3

emissions and gas-particle partitioning (Li et al., 2014; Meng et al., 2011; Plessow et al., 2005; Walker et al., 2004; Zbieranowski and Aherne, 2012). Day et al. (2012) previously suggested that trapping of regional NH_3 emissions in a shallow winter boundary layer can produce elevated surface concentrations. The BAO tower observations in Fig. 5a support this hypothesis, as concentrations are elevated near the surface but fall off quickly at heights greater than 10-20 m. Evidence of winter temperature inversions is present even in the average winter temperature profile shown in Fig. 5b.

Several long-term measurements have shown a strong correlation between NH_3 concentration and ambient temperature, due to enhanced NH_3 emissions from soil and volatilization from NH_4NO_3 particulate matter (Bari et al., 2003; Ianniello et al., 2010; Lin et al., 2006; Meng et al., 2011). Almost no correlation ($R^2=0.02$) between NH_3 concentration and temperature was observed at 1 m height in the current study; higher correlation ($R^2=0.65$) was found at the top of the tower (Fig. S3a). The correlation coefficients increase substantially with height (Fig. S3b), particularly above 50 m, suggesting that temperature might influence ambient NH_3 concentrations at this location at higher altitude but is not a dominant factor at the surface (Fig. S3b). This pattern likely reflects greater vertical mixing during warmer periods, as discussed above. In order to investigate the possible influence of changes in NH_4NO_3 aerosol-gas partitioning on vertical NH_3 concentration profiles, thermodynamic simulations were performed using the ISORROPIA II model (Fountoukis and Nenes, 2007) (Fig. S4). Model inputs included BAO site URG denuder/filter-pack surface measurements of key species (gaseous NH_3 and HNO_3 and $\text{PM}_{2.5}$ NH_4^+ , NO_3^- , and SO_4^{2-}) and measurements of temperature and relative

humidity at each tower measurement height. Because vertical differences in temperature and relative humidity were generally small, little change was predicted with height in the thermodynamic partitioning of the $\text{NH}_3\text{-HNO}_3\text{-NH}_4\text{NO}_3$ system. Consequently, a shift in partitioning toward the particle phase as temperatures cool at higher altitudes appears not to account for much of the observed decrease in NH_3 concentration with height. For this location and for the lowest 300 m of the atmosphere, the vertical thermal structure of the atmosphere and associated mixing, ambient dilution, and NH_3 surface deposition appear to be the major factors determining vertical distributions of atmospheric NH_3 .

3.3 Comparison with satellite observations

Several recent studies have used surface NH_3 measurements to evaluate or improve remote sensing techniques for retrieving NH_3 concentrations and determining distributions (Heald et al., 2012; Pinder et al., 2011; Zhu et al., 2013; Van Damme et al., 2015). The first version of the IASI- NH_3 data set has been evaluated against model simulations over Europe and has demonstrated consistency between model output and satellite retrieval derived NH_3 concentrations (Van Damme et al., 2014). These initial validation steps highlighted the need to expand the NH_3 monitoring network to achieve a more complete validation of the NH_3 satellite observations (Van Damme et al., 2015). The comparison here is a contribution to that effort and benefits from a relatively high spatial density of monitoring sites in a region with substantial NH_3 emission and concentration gradients.

In Fig. 6a IASI-retrieved column distributions averaged over the ground-based measurement period from 2012 to 2015 are compared with the Radiello passive NH_3

525 surface concentration measurements in northeastern Colorado. Only IASI observations
526 with a relative error below 100% or an absolute error below 5×10^{15} molec/cm² were used
527 for comparison in the latitude range from 39°N to 42°N and longitude range from 102°W
528 to 106°W. This combined filtering using relative and absolute thresholds on the error avoids
529 introducing a bias when averaging and results in considering 98.5% of the IASI cloud-free
530 morning observations for this area. Overall, the IASI observations and Radiello passive
531 measurements show similar spatial patterns. The IASI columns exceed 2×10^{16} molec/cm²
532 around the KY site and decrease moving away from concentrated agricultural areas.

533
534 In order to further explore the temporal concentration variability, including the postulated
535 contributions from wildfire to local ambient NH₃ concentrations, averages of IASI
536 measurements (based on weekly or bi-weekly Radiello passive sampling periods) above
537 the FC_W site are shown in Fig. 7. In general, similar temporal trends are found between
538 the Radiello passive measurements (blue) and IASI observations (red). Elevated NH₃
539 concentrations during the High Park Fire period in June 2012 are seen in both the satellite
540 and surface measurements. It is also interesting to note the relatively high IASI-NH₃ total
541 column measured at the beginning of June 2011 (8.5×10^{15} molec/cm²), which could be
542 linked with transported wildfire plumes at higher altitude (Fig. S5) not captured by surface
543 measurements.

544
545 The similar spatial and temporal patterns captured show the respective consistency of the
546 IASI measurements and the Radiello network to monitor regional NH₃ variations in
547 northeast Colorado. The passive measurements provide an accurate, long-term record of

spatial variability and surface concentration trends while the IASI satellite NH₃ columns provide higher time resolution snapshots of conditions over the region, including plumes elevated above the surface.

3.4 Comparison with CAMx Model Simulations

Simulations with CAMx version 6.1 were performed with two-way nested domains and horizontal grid size resolutions of 36 km, 12 km, and 4 km (Fig. S6). The outermost domain includes the continental U.S., southern Canada, and northern Mexico, the 12-km domain extends over the western states, and the 4 km domain extends over Colorado, Wyoming and Utah. The Weather Research & Forecasting Model (WRF), Advanced Research WRF (ARW) v3.5.1, was used to develop meteorological inputs to the air quality model (Skamarock et al., 2005). The input meteorological data represent conditions as they occurred in 2011. A performance evaluation of the WRF simulations was conducted by The University of North Carolina at Chapel Hill (Three-State Air Quality Modeling Study (3SAQS) – Weather Research Forecast 2011 Meteorological Model Application/Evaluation available at: http://vibe.cira.colostate.edu/wiki/Attachments/Modeling/3SAQS_2011_WRF_MPE_v05_Mar2015.pdf). Model performance was evaluated by the Intermountain West Data Warehouse team (Adelman et al., 2015). The model met performance standards as recommended by the U.S. EPA for regulatory photochemical modeling purposes (https://www3.epa.gov/scram001/guidance/guide/Draft_O3-PM-RH_Modeling_Guidance-2014.pdf). In general, model performance statistics for ambient concentrations of ozone and many individual species of fine particles fell within the

recommended ranges. However, concentrations of organic and elemental carbon (two particulate matter species) are over-predicted by the model and performance criteria falls outside the recommended range. Additionally, modeled particulate NO_3^- concentrations are over-predicted in the winter, and under-predicted in the summer in most locations. Model performance with respect to NH_3 can be best evaluated using the measurement data presented in this report.

The Sparse Matrix Operator Kernel Emissions (SMOKE) processing system (<https://www.cmascenter.org/smoke/documentation/3.1/html/>; Houyoux et al., 2000) was used to prepare the emissions inventory data in a format that reflects the spatial, temporal, and chemical speciation parameters required by CAMx. The emissions inventory is based on the 2011 NEI v1 (http://www.epa.gov/ttn/chief/net/2011nei/2011_nei_tsdv1_draft2_june2014.pdf).

Important updates to the 2011 NEI included a detailed oil and gas inventory, and the spatial allocation of livestock emissions using latitude/longitude location data of livestock facilities (IWDW-WAQS). Boundary conditions were developed using the Model for Ozone and Related chemical Tracers (MOZART) and represent the 2011 modeling period (Emmons et al., 2010).

Fig. 6b illustrates an evaluation of CAMx simulated NH_3 concentrations both spatially and across time. Generally speaking, CAMx reasonably reproduces average observed NH_3 in the northeastern plains of Colorado, with a model/measurement ratio of 91% averaged across all measurement locations. This is a much closer match than a separate 12 km

594 resolution CMAQ summer 2014 model comparison to surface passive ammonia
595 measurements (including some of the observations collected in the current study) reported
596 by Battye et al. (2016), who found that the average measured concentration was 2.7 times
597 higher than the modeled concentration. Despite the better average comparison of
598 measurements with the CAMx prediction reported here, however, the CAMx simulation
599 tends to over-estimate concentrations near major NH₃ sources (e.g., at the KY monitoring
600 site), while under-estimating NH₃ concentrations at sites further away from feedlot
601 locations (Fig. 8). Across our measurement locations, the model performance is best at GY,
602 a site surrounded by, but not immediately adjacent to, large NH₃ sources. The modest
603 overestimation of NH₃ concentration at the KY site is likely an artifact of model resolution
604 and the assumption that emissions are immediately and homogeneously dispersed
605 throughout the grid cell in which they are emitted. A model-measurement mismatch
606 moving farther away from NH₃ source locations could result from a number of factors,
607 including smaller and/or non-agricultural sources (e.g., suburban N-fertilization or
608 transportation) under-represented in the emissions inventory, possible over-estimation of
609 NH₃ deposition in the model, which does not account for the bidirectional nature of NH₃
610 exchange with the surface, or a tendency for the model to more actively move surface NH₃
611 emissions aloft during downwind transport than occurs in the real atmosphere.

612
613 Fig. 9 shows both measured (measurements taken in 2012) and modeled (2011) vertical
614 concentrations of NH₃ at the BAO tower location. Although these comparisons are for two
615 adjacent years, the results presented earlier demonstrate that seasonal average
616 concentrations across the region are typically similar from year to year. Modeled vertical

NH₃ concentrations are reported from the lowest 6 levels of the model, up to approximately 325 m above the surface. The model height represented by the value plotted on the y-axis in Fig. 9a represents the top of the layer from which the corresponding concentration is reported (i.e. the surface or lowest model layer is reported at 24 meters – the approximate height of the surface layer). Model layer height is based on the meteorological model and modeled pressure and is not fixed (http://vibe.cira.colostate.edu/wiki/Attachments/Modeling/3SAQS_2011_WRF_MPE_v05Mar2015.pdf). The vertical concentrations are homogeneous within each model layer. Therefore, the model is not able to capture the detailed vertical pattern shown from 0 to 10 to 20 meters by the observations. The model-measurement comparisons of vertical profiles demonstrate a significant under-prediction by the model at all elevations in all four seasons. The under-prediction at the surface is consistent with the observation above that the model tends to under-estimate NH₃ concentrations farther from the major regional feedlot sources. The fact that the model also under-predicts NH₃ aloft suggests that the surface mismatch is not simply a result of excess vertical transport of NH₃ in the model. Model vertical NH₃ concentration profiles normalized for surface concentration are shown in Fig. 9b and compared to similarly normalized measurements. These profiles suggest that the model does a reasonable job of capturing the shape of the observed vertical concentration gradient, although the relative concentration decrease with height in the model is a bit stronger than observed via passive sampler measurements in each season.

4 Conclusions

Six years of passive sampler measurements revealed strong spatial differences in NH_3 concentrations in northeastern Colorado. Summer average weekly NH_3 concentrations ranged from $2.7 \mu\text{g}/\text{m}^3$ to $42.7 \mu\text{g}/\text{m}^3$. The lowest average NH_3 concentration always occurred at a remote prairie site, while average NH_3 concentrations nearly a factor of 15 greater were observed at a site near a large animal feeding operation. Based on six years of available data, no significant regional long-term trends were detected in NH_3 concentrations at 6 of the 9 study sites, consistent with similar seasonal meteorological conditions and relative stability in regional livestock headcounts over the period. Two sites near animal feeding operations (GY and KY) showed evidence of an increasing NH_3 concentration trend, while a decreasing trend was evident at a 3rd site (BH). Further effort is warranted to see whether changes in local animal feeding operations might explain these trends. The NH_3 concentration levels observed in this study provide an important reference point for evaluating the success of future efforts to mitigate regional NH_3 emissions through voluntary implementation of BMPs as part of a strategy to reduce nitrogen deposition levels and impacts in nearby Rocky Mountain National Park.

Measurement of NH_3 at the BAO meteorological tower near Erie, Colorado provide the first long-term insights into vertical gradients of NH_3 concentrations in the region and some of the first long-term measurements of this type anywhere in the world. A general pattern of decreasing NH_3 concentrations with height above 10 m was observed in all seasons, as was a decreasing concentration below 10 m height. The lowest average concentrations were observed in winter at the surface along with a steeper vertical concentration gradient. Higher average concentrations were observed in summer at all altitudes along with a

shallower vertical concentration gradient. Surface deposition, vertical dilution, and the formation of thermal inversions that limit the vertical mixing of regional, surface-based NH_3 emissions appear to have greater influence than temperature and humidity-driven changes in NH_4NO_3 gas-particle partitioning on the observed vertical concentration profiles.

Comparison of measured NH_3 spatial distributions with IASI satellite retrieved NH_3 columns reveals that both monitoring techniques capture similar spatial and temporal variability in northeastern Colorado. These comparisons lend additional weight to the growing body of evidence suggesting that satellite retrievals of NH_3 columns can provide useful information about spatial and temporal concentration variability of this key species, even in regions with strong sources and sharp spatial concentration gradients. Some temporal differences between satellite and *in situ* measurements at the FC_W site appear to reflect NH_3 in elevated wildfire plumes that are observed from the satellite but are not sampled at the surface.

Measured spatial distributions of NH_3 concentrations also provide a good basis for comparison to regional air quality model simulations. A comparison with CAMx simulations finds that the model captures average NH_3 concentrations across the study, but tends to over-predict concentrations close to sources and under-predict concentrations at locations further away. A comparison of measured and modeled vertical profiles in a non-source region reveals an under-prediction of modeled NH_3 from the surface up to 300 m in all seasons. The mismatch aloft provides evidence that the difficulty for the model in

reproducing surface observations away from sources is not a simple result of excess vertical mixing of NH_3 emissions in the model. Rather, the model emission inventory may be missing or under-predicting smaller or non-agricultural NH_3 sources or, perhaps more likely, the model may be over-predicting surface NH_3 deposition due to the absence of bidirectional treatment of NH_3 atmosphere-surface exchange. Although additional research is definitely needed, we expect the NH_3 concentrations and spatial/vertical differences presented here to be useful in constraining future simulated concentrations of atmospheric NH_3 in chemical transport models.

Acknowledgements

Primary funding for this work was provided by the USDA through the Colorado State University Agriculture Experiment Station (project COL00699). Additional support and equipment were provided by the National Park Service. The authors are grateful to the many people who helped to make these measurements possible, especially allowing access to the sampling sites. The authors thank Bonne Ford, Arsineh Hecobian and Liye Zhu from Colorado State University for their helpful suggestions. The authors thank Daniel Wolfe and Bruce Bartram from the BAO tower for assistance with the tower measurements. The authors also thank Tom Moore from Western States Air Resources Council and Rodger Ames from Cooperative Institute for Research in the Atmosphere for modeling help. Simon Whitburn is grateful for his Ph.D. grant (Boursier FRIA) to the “Fonds pour la Formation à la Recherche dans l’Industrie et dans l’Agriculture” of Belgium. L. C. is a Research Associate (Chercheur Qualifié) with the Belgian F.R.S.-FNRS. The data included in this

707 paper are maintained at Colorado State University and will be available for a minimum of
708 5 years after publication by contacting collett@atmos.colostate.edu.

References

- Adelman, Z., Shanker, U., Yang, D., and Morris, R.: Three-State Air Quality Modeling Study CAMx Photochemical Grid Model Draft Model Performance Evaluation Simulation Year 2011, University of North Carolina at Chapel Hill and ENVIRON International Corporation, Novato, CA. June, 2015.
- Aneja, V. P., Roelle, P. A., Murray, G. C., Southerland, J., Erisman, J. W., Fowler, D., Asman, W. A. H., and Patni, N.: Atmospheric nitrogen compounds II: emissions, transport, transformation, deposition and assessment, *Atmospheric Environment*, 35, 1903-1911, 2001.
- Aneja, V. P., Schlesinger, W. H., Nyogi, D., Jennings, G., Gilliam, W., Knighton, R. E., Duke, C. S., Blunden, J., and Krishnan, S.: Emerging national research needs for agricultural air quality, *Eos, Transactions American Geophysical Union*, 87, 25-29, 2006.
- Asman, W. A. H., Sutton, M. A., and SchjØrring, J. K.: Ammonia: emission, atmospheric transport and deposition, *New Phytologist*, 139, 27-48, 1998.
- Bari, A., Ferraro, V., Wilson, L. R., Luttinger, D., and Husain, L.: Measurements of gaseous HONO, HNO₃, SO₂, HCl, NH₃, particulate sulfate and PM_{2.5} in New York, NY, *Atmospheric Environment*, 37, 2825-2835, 2003.
- Bash, J. O., Cooter, E. J., Dennis, R. L., Walker, J. T., and Pleim, J. E.: Evaluation of a regional air-quality model with bidirectional NH₃ exchange coupled to an agroecosystem model, *Biogeosciences*, 10, 1635-1645, 2013.
- Battye, W. H., Bray, C. D., Aneja, V. P., Tong, D., Lee, P., and Tang, Y.: Evaluating ammonia (NH₃) predictions in the NOAA National Air Quality Forecast Capability

(NAQFC) using in situ aircraft, ground-level, and satellite measurements from the DISCOVER-AQ Colorado campaign, *Atmospheric Environment*, 140, 342-351, 2016.

Bauer, S. E., Tsigaridis, K., and Miller, R.: Significant atmospheric aerosol pollution caused by world food cultivation, *Geophysical Research Letters*, 43, 5394-5400, 2016.

Beem, K. B., Raja, S., Schwandner, F. M., Taylor, C., Lee, T., Sullivan, A. P., Carrico, C. M., McMeeking, G. R., Day, D., and Levin, E.: Deposition of reactive nitrogen during the Rocky Mountain Airborne Nitrogen and Sulfur (RoMANS) study, *Environmental Pollution*, 158, 862-872, 2010.

Benedict, K. B., Carrico, C. M., Kreidenweis, S. M., Schichtel, B., Malm, W. C., and Collett, J. L.: A seasonal nitrogen deposition budget for Rocky Mountain National Park, *Ecological Applications*, 23, 1156-1169, 2013a.

Benedict, K. B., Chen, X., Sullivan, A. P., Li, Y., Day, D., Prenni, A. J., Levin, E., Kreidenweis, S. M., Malm, W. C., and Schichtel, B. A.: Atmospheric concentrations and deposition of reactive nitrogen in Grand Teton National Park, *Journal of Geophysical Research: Atmospheres*, 118, 11,875-811,887, 2013b.

Benedict, K. B., Day, D., Schwandner, F. M., Kreidenweis, S. M., Schichtel, B., Malm, W. C., and Collett, J. L.: Observations of atmospheric reactive nitrogen species in Rocky Mountain National Park and across northern Colorado, *Atmospheric Environment*, 64, 66-76, 2013c.

Benedict, K. B., Prenni, A. J., Carrico, C. M., Sullivan, A. P., Schichtel, B. A., and Collett Jr, J. L.: Enhanced concentrations of reactive nitrogen species in wildfire smoke, *Atmospheric Environment*, 148, 8-15, 2017.

753 Chang, Y., Zou, Z., Deng, C., Huang, K., Collett, J. L., Lin, J., and Zhuang, G.: The
754 importance of vehicle emissions as a source of atmospheric ammonia in the megacity of
755 Shanghai, *Atmospheric Chemistry and Physics*, 16, 3577-3594, 2016.

756 Cisneros, R., Bytnerowicz, A., Schweizer, D., Zhong, S., Traina, S., and Bennett, D. H.:
757 Ozone, nitric acid, and ammonia air pollution is unhealthy for people and ecosystems in
758 southern Sierra Nevada, California, *Environmental Pollution*, 158, 3261-3271, 2010.

759 Clarisse, L., R'Honi, Y., Coheur, P.-F., Hurtmans, D., and Clerbaux, C.: Thermal infrared
760 nadir observations of 24 atmospheric gases, *Geophysical Research Letters*, 38, L10802,
761 2011.

762 Clerbaux, C., Boynard, A., Clarisse, L., George, M., Hadji-Lazaro, J., Herbin, H.,
763 Hurtmans, D., Pommier, M., Razavi, A., and Turquety, S.: Monitoring of atmospheric
764 composition using the thermal infrared IASI/MetOp sounder, *Atmospheric Chemistry and*
765 *Physics*, 9, 6041-6054, 2009.

766 Coheur, P.-F., Clarisse, L., Turquety, S., Hurtmans, D., and Clerbaux, C.: IASI
767 measurements of reactive trace species in biomass burning plumes, *Atmospheric*
768 *Chemistry and Physics*, 9, 5655-5667, 2009.

769 Davidson, C. I., Phalen, R. F., and Solomon, P. A.: Airborne Particulate Matter and Human
770 Health: A Review, *Aerosol Science and Technology*, 39, 737-749, 2005.

771 Day, D. E., Chen, X., Gebhart, K. A., Carrico, C. M., Schwandner, F. M., Benedict, K. B.,
772 Schichtel, B. A., and Collett, J. L.: Spatial and temporal variability of ammonia and other
773 inorganic aerosol species, *Atmospheric Environment*, 61, 490-498, 2012.

774 Eilerman, S. J., Peischl, J., Neuman, J. A., Ryerson, T. B., Aikin, K. C., Holloway, M. W.,
775 Zondlo, M. A., Golston, L. M., Pan, D., Floerchinger, C., and Herndon, S. C.:

776 Characterization of ammonia, methane, and nitrous oxide emissions from concentrated
777 animal feeding operations in northeastern Colorado, Environmental Science & Technology,
778 2016.

779 Ellis, R. A., Jacob, D. J., Sulprizio, M. P., Zhang, L., Holmes, C. D., Schichtel, B. A., Blett,
780 T., Porter, E., Pardo, L. H., and Lynch, J. A.: Present and future nitrogen deposition to
781 national parks in the United States: critical load exceedances, Atmospheric Chemistry and
782 Physics, 13, 9083-9095, 2013.

783 Emmons, L., Walters, S., Hess, P., Lamarque, J.-F., Pfister, G., Fillmore, D., Granier, C.,
784 Guenther, A., Kinnison, D., and Laepple, T.: Description and evaluation of the Model for
785 Ozone and Related chemical Tracers, version 4 (MOZART-4), Geoscientific Model
786 Development, 3, 43-67, 2010.

787 EPA, U.: Guidance on the use of models and other analyses for demonstrating attainment
788 of air quality goals for ozone, PM_{2.5}, and regional haze, EPA-454/B07-002, 2007.

789 EPA, U.: Air Quality Modeling Final Rule Technical Support Document, EPA Office of
790 Air Quality Planning and Standards 2011.

791 Fountoukis, C., and Nenes, A.: ISORROPIA II: a computationally efficient
792 thermodynamic equilibrium model for $K^+ - Ca^{2+} - Mg^{2+} - NH_4^+ - Na^+ - SO_4^{2-} - NO_3^- - Cl^- - H_2O$
793 aerosols, Atmospheric Chemistry and Physics, 7, 4639-4659, 2007.

794 Fowler, D., Pitcairn, C. E. R., Sutton, M. A., Flechard, C., Loubet, B., Coyle, M., and
795 Munro, R. C.: The mass budget of atmospheric ammonia in woodland within 1 km of
796 livestock buildings, Environmental Pollution, 102, 343-348, 1998.

797 Gilbert, R. O.: Statistical methods for environmental pollution monitoring, John Wiley &
798 Sons, 1987.

799 Hand, J., Schichtel, B., Malm, W., and Pitchford, M.: Particulate sulfate ion concentration
800 and SO₂ emission trends in the United States from the early 1990s through 2010,
801 Atmospheric Chemistry and Physics, 12, 10353-10365, 2012.

802 Heald, C. L., Collett Jr, J., Lee, T., Benedict, K., Schwandner, F., Li, Y., Clarisse, L.,
803 Hurtmans, D., Van Damme, M., and Clerbaux, C.: Atmospheric ammonia and particulate
804 inorganic nitrogen over the United States, Atmospheric Chemistry and Physics, 12, 10295-
805 10312, 2012.

806 Hertel, O., Skjøth, C. A., Løfstrøm, P., Geels, C., Frohn, L. M., Ellermann, T., and Madsen,
807 P. V.: Modelling Nitrogen Deposition on a Local Scale—A Review of the Current State of
808 the Art, Environmental Chemistry, 3, 317-337, 2006.

809 Horii, C. V., William Munger, J., Wofsy, S. C., Zahniser, M., Nelson, D., and Barry
810 McManus, J.: Atmospheric reactive nitrogen concentration and flux budgets at a
811 Northeastern U.S. forest site, Agricultural and Forest Meteorology, 136, 159-174, 2006.

812 Houyoux, M., Vukovich, J., Brandmeyer, J., Seppanen, C., and Holland, A.: Sparse Matrix
813 Operator Kernel Emissions Modeling System-SMOKE User Manual, Prepared by MCNC-
814 North Carolina Supercomputing Center, Environmental Programs, Research Triangle Park,
815 NC, 2000.

816 Ianniello, A., Spataro, F., Esposito, G., Allegrini, I., Rantica, E., Ancora, M., Hu, M., and
817 Zhu, T.: Occurrence of gas phase ammonia in the area of Beijing (China), Atmospheric
818 Chemistry and Physics, 10, 9487-9503, 2010.

819 Ianniello, A., Spataro, F., Esposito, G., Allegrini, I., Hu, M., and Zhu, T.: Chemical
820 characteristics of inorganic ammonium salts in PM_{2.5} in the atmosphere of Beijing (China),
821 Atmospheric Chemistry and Physics, 11, 10803-10822, 10.5194/acp-11-10803-2011, 2011.

822 Langridge, J. M., Lack, D., Brock, C. A., Bahreini, R., Middlebrook, A. M., Neuman, J.
823 A., Nowak, J. B., Perring, A. E., Schwarz, J. P., Spackman, J. R., Holloway, J. S., Pollack,
824 I. B., Ryerson, T. B., Roberts, J. M., Warneke, C., de Gouw, J. A., Trainer, M. K., and
825 Murphy, D. M.: Evolution of aerosol properties impacting visibility and direct climate
826 forcing in an ammonia-rich urban environment, *Journal of Geophysical Research:*
827 *Atmospheres*, 117, 2012.

828 Lee, T., Yu, X.-Y., Kreidenweis, S. M., Malm, W. C., and Collett, J. L.: Semi-continuous
829 measurement of PM_{2.5} ionic composition at several rural locations in the United States,
830 *Atmospheric Environment*, 42, 6655-6669, 2008.

831 Lelieveld, J., Evans, J. S., Fnais, M., Giannadaki, D., and Pozzer, A.: The contribution of
832 outdoor air pollution sources to premature mortality on a global scale, *Nature*, 525, 367-
833 371, 2015.

834 Li, Y., Schwandner, F. M., Sewell, H. J., Zivkovich, A., Tigges, M., Raja, S., Holcomb, S.,
835 Molenaar, J. V., Sherman, L., Archuleta, C., Lee, T., and Collett Jr., J. L.: Observations of
836 ammonia, nitric acid, and fine particles in a rural gas production region, *Atmospheric*
837 *Environment*, 83, 80-89, 2014.

838 Li, Y., Schichtel, B. A., Walker, J. T., Schwede, D. B., Chen, X., Lehmann, C. M. B.,
839 Puchalski, M. A., Gay, D. A., and Collett, J. L.: Increasing importance of deposition of
840 reduced nitrogen in the United States, *Proceedings of the National Academy of Sciences*,
841 113, 5874-5879, 2016.

842 Lin, Y.-C., Cheng, M.-T., Ting, W.-Y., and Yeh, C.-R.: Characteristics of gaseous HNO₂,
843 HNO₃, NH₃ and particulate ammonium nitrate in an urban city of Central Taiwan,
844 *Atmospheric Environment*, 40, 4725-4733, 2006.

845 Luo, M., Shephard, M. W., Cady-Pereira, K. E., Henze, D. K., Zhu, L., Bash, J. O., Pinder,
846 R. W., Capps, S. L., Walker, J. T., and Jones, M. R.: Satellite observations of tropospheric
847 ammonia and carbon monoxide: Global distributions, regional correlations and
848 comparisons to model simulations, *Atmospheric Environment*, 106, 262-277, 2015.

849 Malm, W. C., Schichtel, B. A., Barna, M. G., Gebhart, K. A., Rodriguez, M. A., Collett, J.
850 L., Carrico, C. M., Benedict, K. B., Prenni, A. J., and Kreidenweis, S. M.: Aerosol species
851 concentrations and source apportionment of ammonia at Rocky Mountain National Park,
852 *Journal of the Air & Waste Management Association*, 63, 1245-1263, 2013.

853 Malm, W. C., Rodriguez, M. A., Schichtel, B. A., Gebhart, K. A., Thompson, T. M., Barna,
854 M. G., Benedict, K. B., Carrico, C. M., and Collett, J. L.: A hybrid modeling approach for
855 estimating reactive nitrogen deposition in Rocky Mountain National Park, *Atmospheric*
856 *Environment*, 126, 258-273, 2016.

857 Marchetto, A., Rogora, M., and Arisci, S.: Trend analysis of atmospheric deposition data:
858 A comparison of statistical approaches, *Atmospheric Environment*, 64, 95-102, 2013.

859 Massman, W. J.: A review of the molecular diffusivities of H₂O, CO₂, CH₄, CO, O₃, SO₂,
860 NH₃, N₂O, NO, and NO₂ in air, O₂ and N₂ near STP, *Atmospheric Environment*, 32, 1111-
861 1127, 1998.

862 Meng, Z., Lin, W., Jiang, X., Yan, P., Wang, Y., Zhang, Y., Jia, X., and Yu, X.:
863 Characteristics of atmospheric ammonia over Beijing, China, *Atmospheric Chemistry and*
864 *Physics*, 11, 6139-6151, 2011.

865 Müller, M., Mikoviny, T., Feil, S., Haidacher, S., Hanel, G., Hartungen, E., Jordan, A.,
866 Märk, L., Mutschlechner, P., and Schotchkowsky, R.: A compact PTR-ToF-MS instrument

867 for airborne measurements of volatile organic compounds at high spatiotemporal resolution,
868 *Atmospheric Measurement Techniques*, 7, 3763-3772, 2014.

869 Nowak, J., Neuman, J., Bahreini, R., Middlebrook, A., Holloway, J., McKeen, S., Parrish,
870 D., Ryerson, T., and Trainer, M.: Ammonia sources in the California South Coast Air Basin
871 and their impact on ammonium nitrate formation, *Geophysical Research Letters*, 39, 2012.

872 Pan, Y., Wang, Y., Tang, G., and Wu, D.: Wet and dry deposition of atmospheric nitrogen
873 at ten sites in Northern China, *Atmospheric Chemistry and Physics*, 12, 6515-6535, 2012.

874 Park, R. J., Jacob, D. J., Kumar, N., and Yantosca, R. M.: Regional visibility statistics in
875 the United States: Natural and transboundary pollution influences, and implications for the
876 Regional Haze Rule, *Atmospheric Environment*, 40, 5405-5423, 2006.

877 Parry, M. L., Canziani, O. F., Palutikof, J. P., van der Linden, P. J., and Hanson, C. E.:
878 IPCC, 2007: climate change 2007: impacts, adaptation and vulnerability. Contribution of
879 working group II to the fourth assessment report of the intergovernmental panel on climate
880 change, in, Cambridge University Press, Cambridge, 2007.

881 Paulot, F., Jacob, D. J., and Henze, D. K.: Sources and processes contributing to nitrogen
882 deposition: an adjoint model analysis applied to biodiversity hotspots worldwide,
883 *Environmental Science & Technology*, 47, 3226-3233, 2013.

884 Pinder, R. W., Walker, J. T., Bash, J. O., Cady-Pereira, K. E., Henze, D. K., Luo, M.,
885 Osterman, G. B., and Shephard, M. W.: Quantifying spatial and seasonal variability in
886 atmospheric ammonia with in situ and space-based observations, *Geophysical Research*
887 *Letters*, 38, L04802, 2011.

888 Pleim, J. E., Bash, J. O., Walker, J. T., and Cooter, E. J.: Development and evaluation of
889 an ammonia bidirectional flux parameterization for air quality models, *Journal of*
890 *Geophysical Research: Atmospheres*, 118, 3794-3806, 2013.

891 Plessow, K., Spindler, G., Zimmermann, F., and Matschullat, J.: Seasonal variations and
892 interactions of N-containing gases and particles over a coniferous forest, Saxony, Germany,
893 *Atmospheric Environment*, 39, 6995-7007, 2005.

894 Prenni, A., Chen, X., Hecobian, A., Kreidenweis, S., Collett, J., and Schichtel, B.:
895 Measurements of gas phase reactive nitrogen during two wildfires in Colorado, AGU Fall
896 Meeting Abstracts, 2012, 0618.

897 Prenni, A., Levin, E., Benedict, K., Sullivan, A., Schurman, M., Gebhart, K., Day, D.,
898 Carrico, C., Malm, W., and Schichtel, B.: Gas-phase reactive nitrogen near Grand Teton
899 National Park: Impacts of transport, anthropogenic emissions, and biomass burning,
900 *Atmospheric Environment*, 89, 749-756, 2014.

901 Puchalski, M. A., Sather, M. E., Walker, J. T., Lehmann, C. M., Gay, D. A., Mathew, J.,
902 and Robarge, W. P.: Passive ammonia monitoring in the United States: Comparing three
903 different sampling devices, *Journal of Environmental Monitoring*, 13, 3156-3167, 2011.

904 Pul, A., Hertel, O., Geels, C., Dore, A., Vieno, M., Jaarsveld, H., Bergström, R., Schaap,
905 M., and Fagerli, H.: Modelling of the Atmospheric Transport and Deposition of Ammonia
906 at a National and Regional Scale, in: *Atmospheric Ammonia*, edited by: Sutton, M., Reis,
907 S., and Baker, S. H., Springer Netherlands, 301-358, 2009.

908 Reche, C., Viana, M., Pandolfi, M., Alastuey, A., Moreno, T., Amato, F., Ripoll, A., and
909 Querol, X.: Urban NH₃ levels and sources in a Mediterranean environment, *Atmospheric*
910 *Environment*, 57, 153-164, 2012.

911 Rodriguez, M. A., Barna, M. G., Gebhart, K. A., Hand, J. L., Adelman, Z. E., Schichtel, B.
912 A., Collett Jr, J. L., and Malm, W. C.: Modeling the fate of atmospheric reduced nitrogen
913 during the Rocky Mountain Atmospheric Nitrogen and Sulfur Study (RoMANS):
914 Performance evaluation and diagnosis using integrated processes rate analysis,
915 Atmospheric Environment, 45, 223-234, 2011.

916 Schiferl, L. D., Heald, C. L., Nowak, J. B., Holloway, J. S., Neuman, J. A., Bahreini, R.,
917 Pollack, I. B., Ryerson, T. B., Wiedinmyer, C., and Murphy, J. G.: An investigation of
918 ammonia and inorganic particulate matter in California during the CalNex campaign,
919 Journal of Geophysical Research: Atmospheres, 119, 1883-1902, 2014.

920 Schwartz, J., and Neas, L. M.: Fine particles are more strongly associated than coarse
921 particles with acute respiratory health effects in schoolchildren, Epidemiology, 11, 6-10,
922 2000.

923 Shelef, M., and Gandhi, H. S.: Ammonia Formation in the Catalytic Reduction of Nitric
924 Oxide. III. The Role of Water Gas Shift, Reduction by Hydrocarbons, and Steam
925 Reforming, Product R&D, 13, 80-85, 1974.

926 Shephard, M., McLinden, C., Cady-Pereira, K., Luo, M., Moussa, S., Leithead, A., Liggio,
927 J., Staebler, R., Akingunola, A., and Makar, P.: Tropospheric Emission Spectrometer (TES)
928 satellite observations of ammonia, methanol, formic acid, and carbon monoxide over the
929 Canadian oil sands: validation and model evaluation, Atmospheric Measurement
930 Techniques, 8, 5189-5211, 2015.

931 Skamarock, W. C., Klemp, J. B., Dudhia, J., Gill, D. O., Barker, D. M., Wang, W., and
932 Powers, J. G.: A description of the advanced research WRF version 2, DTIC Document,
933 2005.

934 Sun, K., Cady - Pereira, K., Miller, D. J., Tao, L., Zondlo, M. A., Nowak, J. B., Neuman,
 935 J., Mikoviny, T., Müller, M., and Wisthaler, A.: Validation of TES ammonia observations
 936 at the single pixel scale in the San Joaquin Valley during DISCOVER - AQ, *Journal of*
 937 *Geophysical Research: Atmospheres*, 120, 5140-5154, 2015.

938 Sutton, M. A., Dragosits, U., Tang, Y. S., and Fowler, D.: Ammonia emissions from non-
 939 agricultural sources in the UK, *Atmospheric Environment*, 34, 855-869, 2000.

940 Sutton, M. A., Erisman, J. W., Dentener, F., and Möller, D.: Ammonia in the environment:
 941 from ancient times to the present, *Environmental Pollution*, 156, 583-604, 2008.

942 Sutton, M. A., Reis, S., Riddick, S. N., Dragosits, U., Nemitz, E., Theobald, M. R., Tang,
 943 Y. S., Braban, C. F., Vieno, M., and Dore, A. J.: Towards a climate-dependent paradigm
 944 of ammonia emission and deposition, *Philosophical Transactions of the Royal Society of*
 945 *London B: Biological Sciences*, 368, 20130166, 2013.

946 Theil, H.: A Rank-Invariant Method of Linear and Polynomial Regression Analysis, in:
 947 Henri Theil's Contributions to Economics and Econometrics, edited by: Raj, B., and Koerts,
 948 J., *Advanced Studies in Theoretical and Applied Econometrics*, Springer Netherlands, 345-
 949 381, 1992.

950 Thompson, T. M., Rodriguez, M. A., Barna, M. G., Gebhart, K. A., Hand, J. L., Day, D.
 951 E., Malm, W. C., Benedict, K. B., Collett, J. L., and Schichtel, B. A.: Rocky Mountain
 952 National Park reduced nitrogen source apportionment, *Journal of Geophysical Research:*
 953 *Atmospheres*, 120, 4370-4384, 2015.

954 Todd, R. W., Cole, N. A., Waldrip, H. M., and Aiken, R. M.: Arrhenius equation for
 955 modeling feedyard ammonia emissions using temperature and diet crude protein, *Journal*
 956 *of Environmental Quality*, 42, 666-671, 2013.

957 USEPA: National Emission Inventory – Ammonia Emissions from Animal Husbandry –
958 Draft Report, US Environmental Protection Agency, Washington, D.C., Jan. 30, 2004,
959 2004.

960 Van Damme, M., Wichink Kruit, R., Schaap, M., Clarisse, L., Clerbaux, C., Coheur, P. F.,
961 Dammers, E., Dolman, A., and Erisman, J.: Evaluating 4 years of atmospheric ammonia
962 (NH_3) over Europe using IASI satellite observations and LOTOS - EUROS model results,
963 Journal of Geophysical Research: Atmospheres, 119, 9549-9566, 2014.

964 Van Damme, M., Clarisse, L., Dammers, E., Liu, X., Nowak, J. B., Clerbaux, C., Flechard,
965 C. R., Galy-Lacaux, C., Xu, W., Neuman, J. A., Tang, Y. S., Sutton, M. A., Erisman, J. W.,
966 and Coheur, P. F.: Towards validation of ammonia (NH_3) measurements from the IASI
967 satellite, Atmospheric Measurement Techniques, 8, 2015.

968 Walker, J. T., Whittall, D. R., Robarge, W., and Paerl, H. W.: Ambient ammonia and
969 ammonium aerosol across a region of variable ammonia emission density, Atmospheric
970 Environment, 38, 1235-1246, 2004.

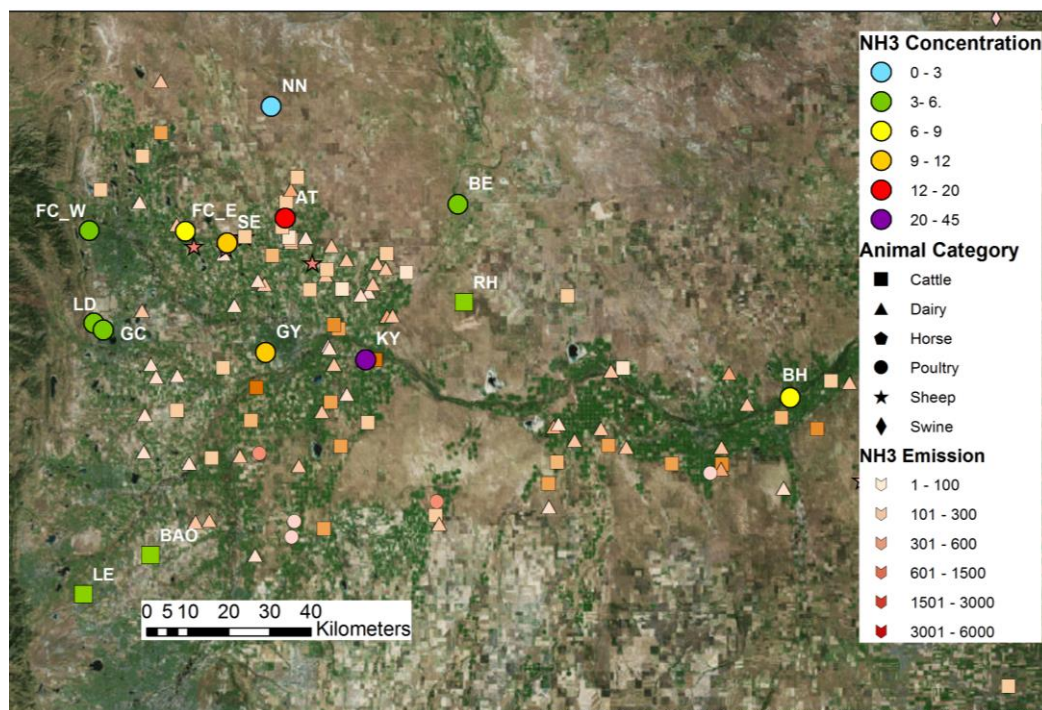
971 Whitburn, S., Van Damme, M., Kaiser, J. W., Van Der Werf, G. R., Turquety, S., Hurtmans,
972 D., Clarisse, L., Clerbaux, C., and Coheur, P.-F.: Ammonia emissions in tropical biomass
973 burning regions: Comparison between satellite-derived emissions and bottom-up fire
974 inventories, Atmospheric Environment, 121, 42-54, 2015.

975 Whitburn, S., Van Damme, M., Clarisse, L., Bauduin, S., Heald, C., Hadji - Lazaro, J.,
976 Hurtmans, D., Zondlo, M., Clerbaux, C., and Coheur, P. F.: A flexible and robust neural
977 network IASI - NH_3 retrieval algorithm, Journal of Geophysical Research: Atmospheres,
978 2016.

979 Zbieranowski, A. L., and Aherne, J.: Spatial and temporal concentration of ambient
980 atmospheric ammonia in southern Ontario, Canada, *Atmospheric Environment*, 62, 441-
981 450, 2012.

982 Zhu, L., Henze, D., Cady - Pereira, K., Shephard, M., Luo, M., Pinder, R., Bash, J., and
983 Jeong, G. R.: Constraining US ammonia emissions using TES remote sensing observations
984 and the GEOS - Chem adjoint model, *Journal of Geophysical Research: Atmospheres*, 118,
985 3355-3368, 2013.

986



988
 989 Fig. 1. NH₃ concentrations (unit: $\mu\text{g}/\text{m}^3$) and feedlot emissions (unit: tons/year) in northeast
 990 Colorado. All sites indicated by circles include at least 3 years of measurements in summer.
 991 NH₃ concentrations at the RH, LE and BAO sites (squares) were only measured in the
 992 summers of 2010, 2011 and 2012, respectively. The predicted annual NH₃ emissions are
 993 calculated based on Eq. 4.

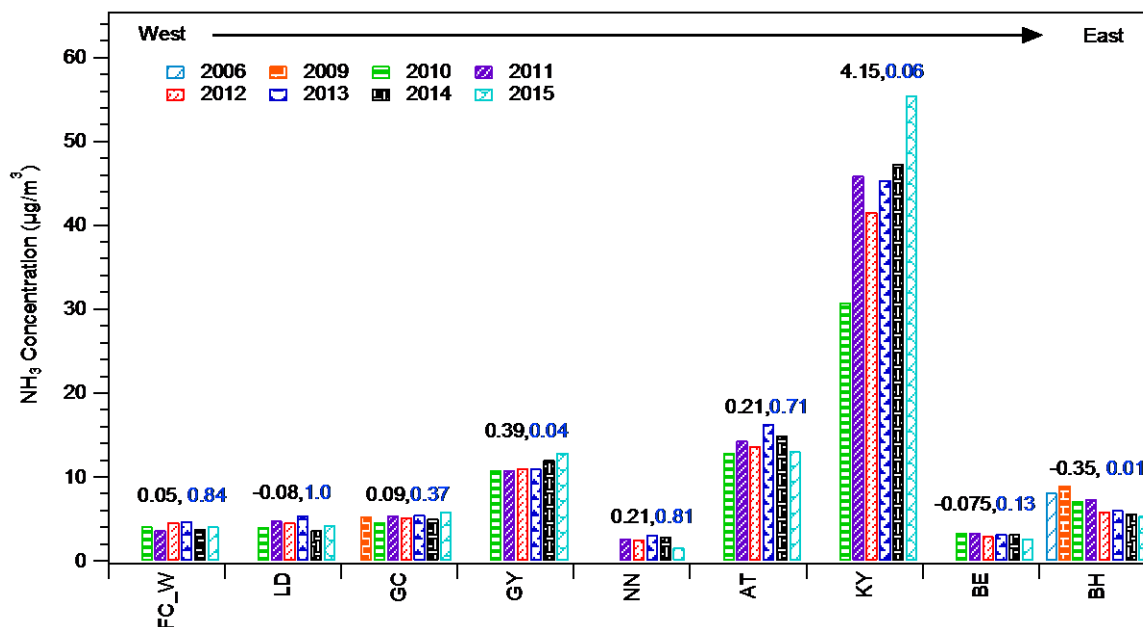
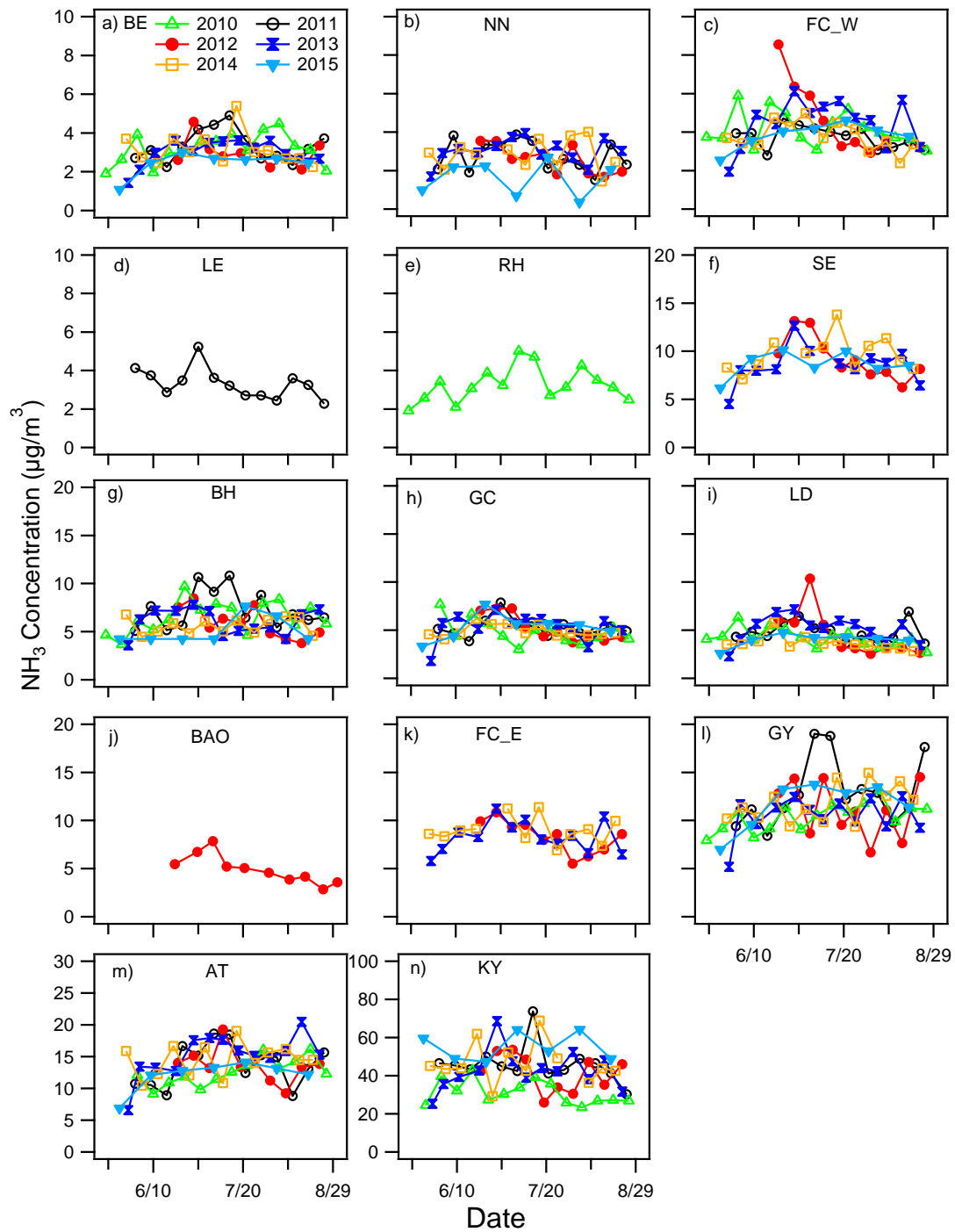


Fig. 2. Average concentrations of NH_3 in each summer (approximately June through August) across the nine sites. In 2006 (07/06-08/10), ambient NH_3 concentrations were sampled by a URG denuder (daily) at the BH site; in 2009 (06/11-08/27) ambient NH_3 concentrations were sampled by a URG denuder (weekly) at the GC and BH sites; in 2010 (06/17-09/02), 2011 (06/16-08/31), 2012 (06/21-08/29), 2013 (06/20-08/29), 2014 (06/19-08/28) and 2015 (06/23-09/01), ambient NH_3 concentrations were all sampled by Radiello NH_3 passive samplers across all the sites. Trend analysis (annual concentration vs. time) was conducted at each site. The slope of the Theil regression and p -value for each site are labeled in black and blue.



1004 Fig. 3. Temporal variations of NH_3 concentrations (unit: $\mu\text{g}/\text{m}^3$) at each site from 2010
 1005 through 2015. Note the differences in the y-axis values.

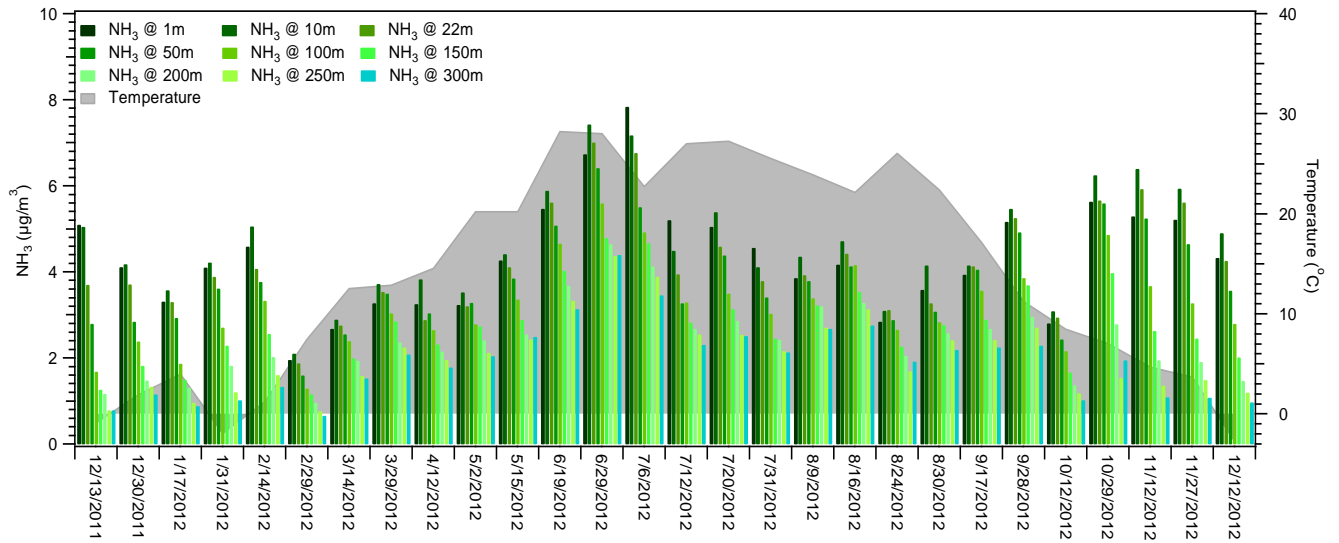


Fig. 4. Time series of vertical distribution of NH_3 concentrations and surface temperature measured at the BAO tower from 12/13/2011 to 01/09/2013.

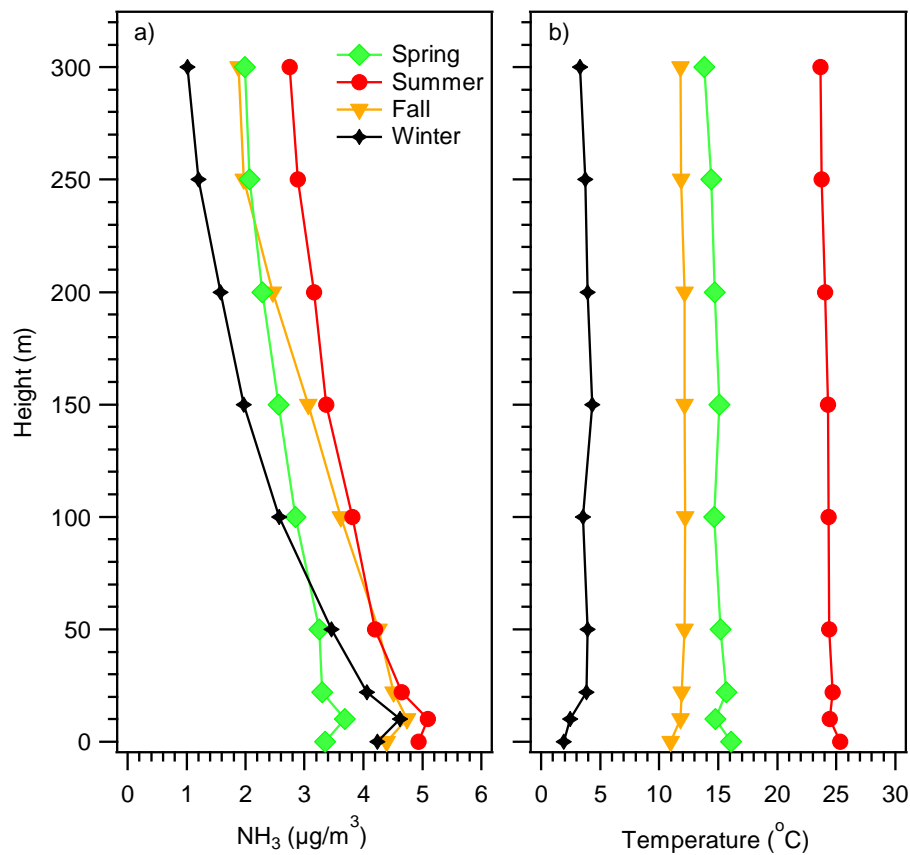


Fig.5. Comparison of seasonal average vertical profiles of (a) NH_3 concentration and (b) temperature measured at the BAO tower from 12/13/2011 to 01/09/2013.

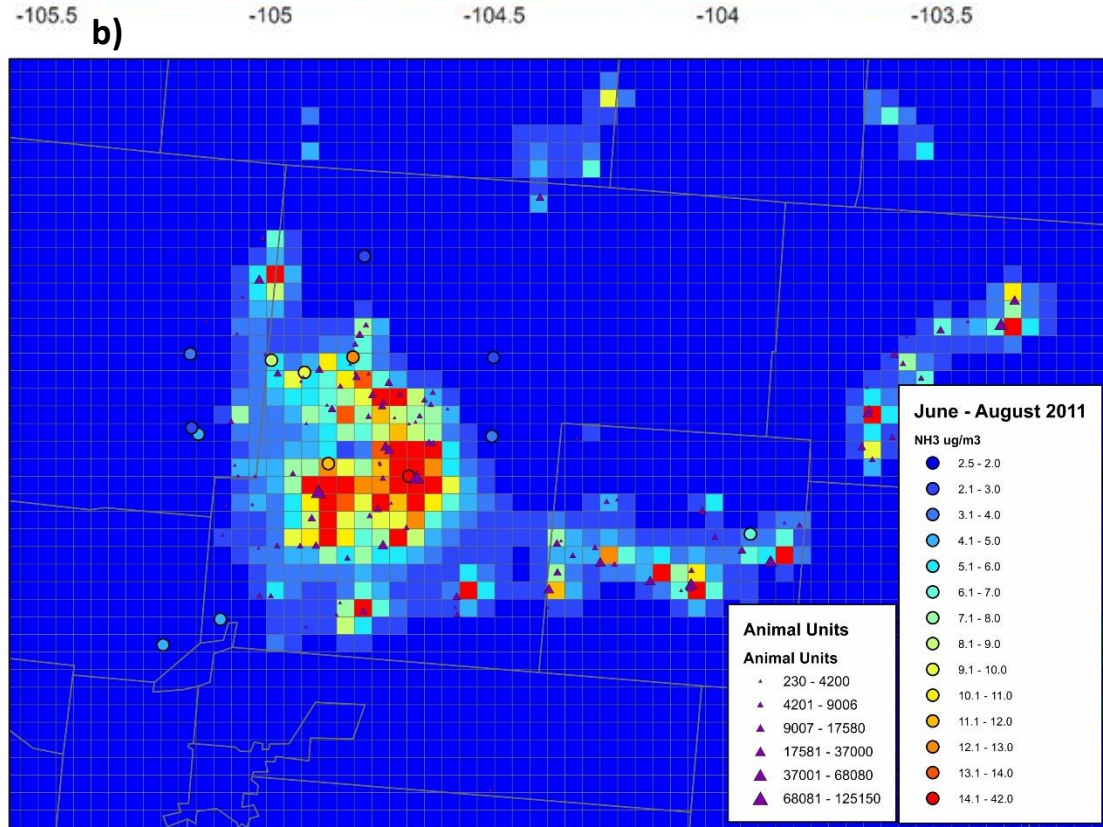
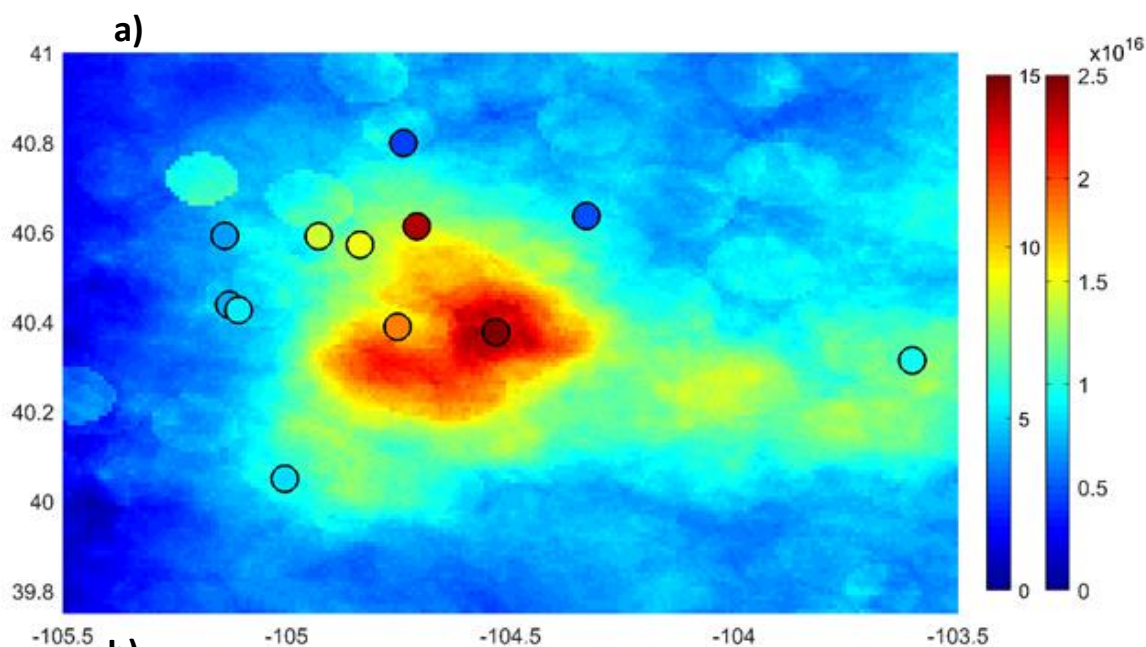


Fig. 6. Comparison of surface NH_3 concentrations with IASI satellite retrievals and CAMx model simulations. a) Radiello passive sampler surface NH_3 concentrations ($\mu\text{g}/\text{m}^3$, left color bar) plotted on top of IASI- NH_3 satellite column retrievals (molec/cm^2 , right color bar), both averaged for the summers of four years (2012-2015). The BAO site was only

sampled *in situ* in the summer of 2012. b) Comparison of measured and modeled NH₃ concentrations in the summer of 2011. The circles correspond to concentrations measured; these are superimposed on the CAMx modeled NH₃ concentration field. Animal units were indicated by the triangles.

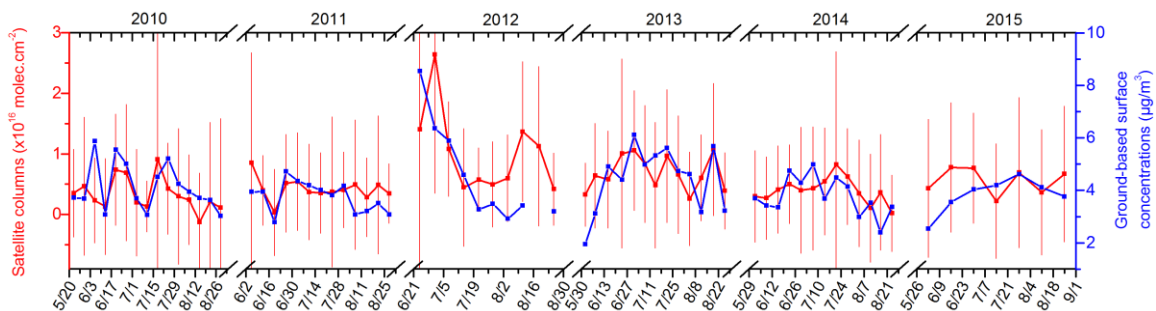


Fig. 7. Time series of (bi-)weekly averaged IASI-NH₃ satellite column (red, $\times 10^{16}$ molec/cm²) and surface concentrations measured by Radiello passive sampler (blue, $\mu\text{g}/\text{m}^3$) at FC_W site. The error bars represent the standard deviation of the mean satellite column retrievals. Please note that the zeros of the two y-axes are not aligned; the data have been aligned for clarity of comparison and to illustrate correlation.

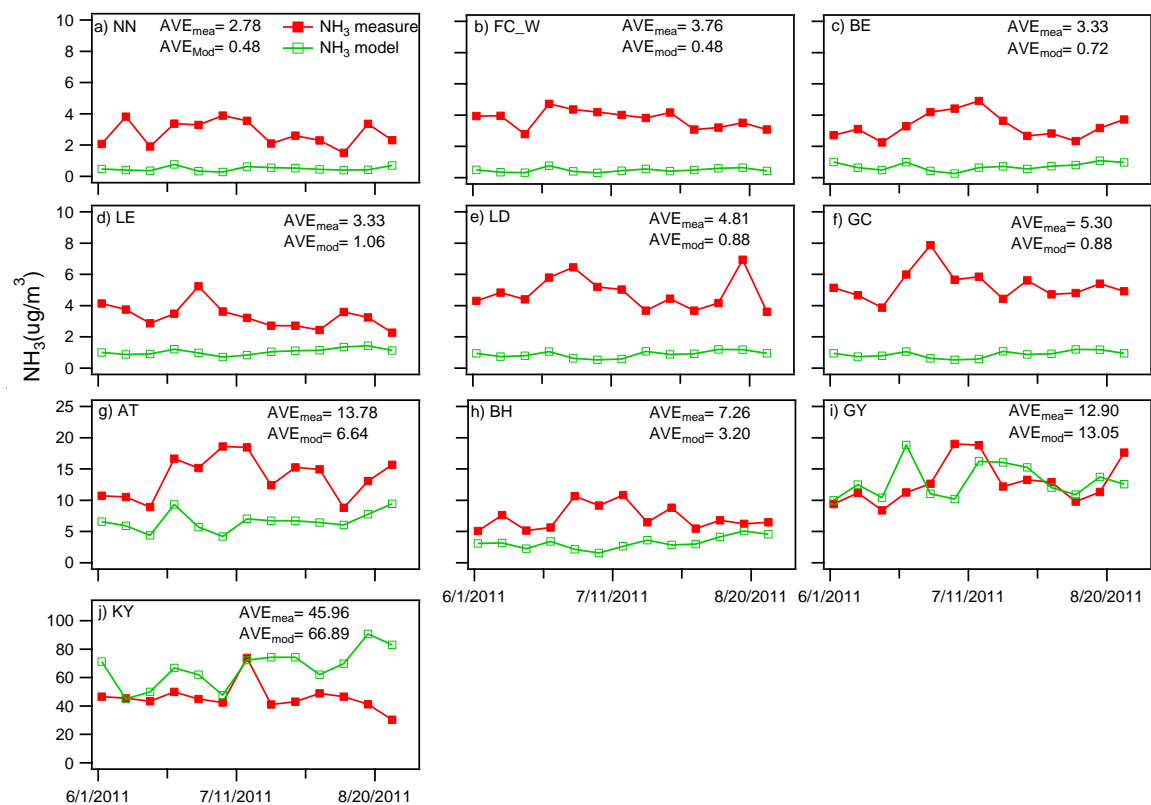


Fig. 8. Time series of weekly NH_3 concentrations measured (red) and modeled (green) in the summer of 2011(06/02/2011-08/31/2011) at all the sites.

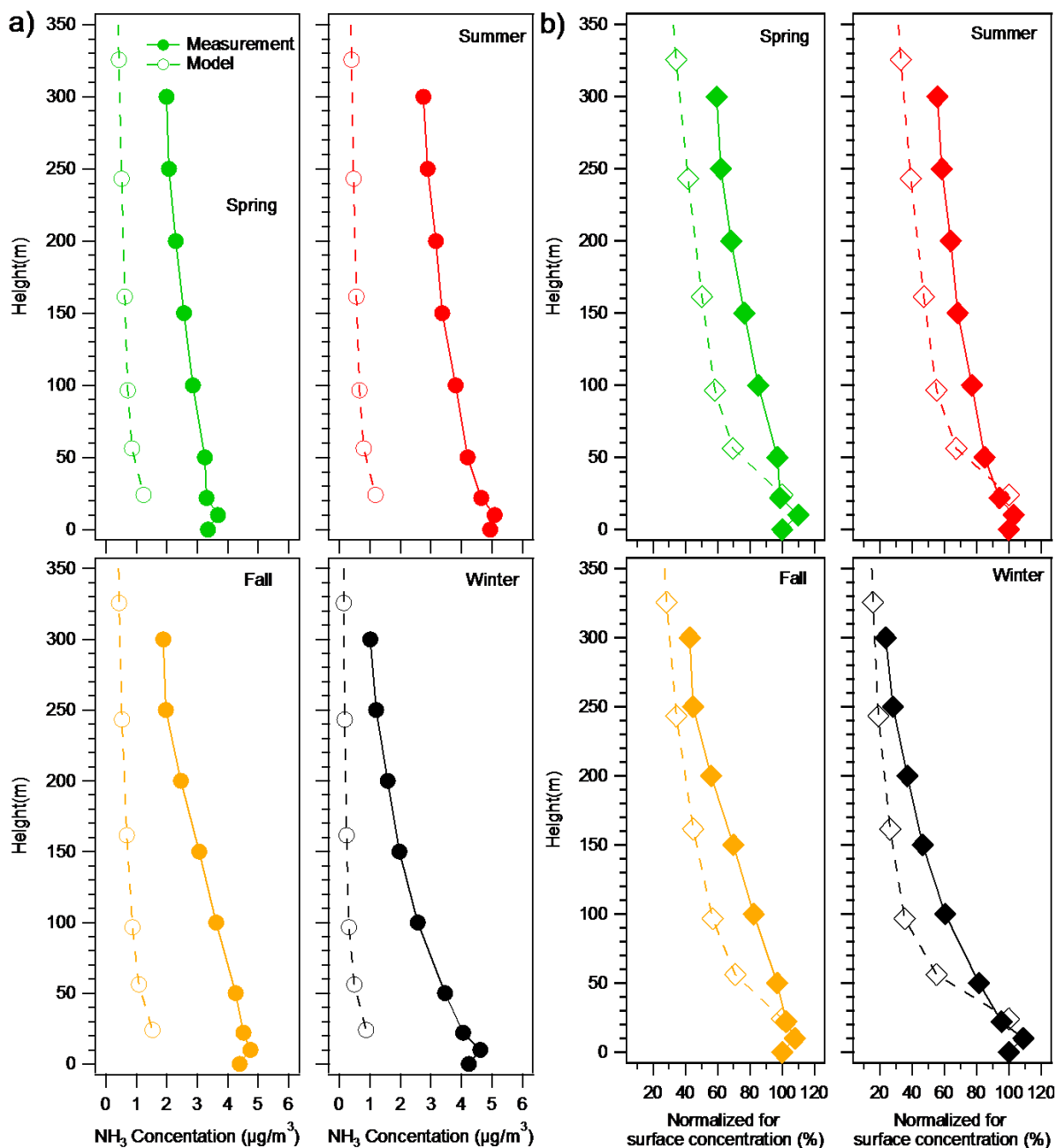


Fig. 9. (a) Comparison of seasonal 2012 NH_3 concentrations ($\mu\text{g}/\text{m}^3$): passive measurements (solid lines) and 2011 CAMx modeling results (dashed lines); (b) comparison of seasonal NH_3 passive measurements normalized by surface concentrations (solid lines) and CAMx modeling results (dashed lines). Each profile is normalized such that the concentration at the lowest level is set to 100.

1037 **Tables**1038 **Table 1. Summary of sampling site locations and dates.**

ID	Site Name	Type	Latitude	Longitude	Elevation(m)	Year*	Sampler type
LE	Louisville	Suburban	39.987	-105.151	1698	11	Passive
FC_W	Fort Collins_West	Suburban	40.589	-105.148	1570	10,11, 12, 13,14,15	Passive/URG
LD	Loveland	Suburban	40.438	-105.127	1582	10,11, 12, 13,14,15	Passive
BAO	BAO Tower	Suburban	40.050	-105.004	1584	12**	Passive/URG
GC	Golf Course	Golf course	40.426	-105.107	1551	10,11, 12, 13,14,15	Passive
FC_E	Fort Collins_East	Suburban- agricultural	40.591	-104.928	1562	12, 13,14	Passive
SE	Severance	Suburban- agricultural	40.572	-104.836	1550	12, 13,14,15	Passive
GY	Greeley	Suburban- agricultural	40.389	-104.751	1492	10,11, 12, 13,14,15	Passive
NN	Nunn	Rural	40.821	-104.701	1644	11,12, 13,14,15	Passive
BE	Briggsdale	Rural	40.635	-104.330	1481	10,11, 12, 13,14,15	Passive
RH	Ranch	Rural	40.473	-104.317	1475	10	Passive
AT	Ault	Rural- agricultural	40.612	-104.709	1514	11,12, 13,14,15	Passive
KY	Kersey	Rural- agricultural	40.377	-104.532	1403	10,11, 12, 13,14,15	Passive
BH	Brush	Rural- agricultural	40.313	-103.602	1286	10,11, 12, 13,14,15	Passive/URG

1039 * Sampling period: 05/20/2010-09/02/2010; 06/02/2011-08/31/2011; 06/21/2012-08/29/2012; 05/30/2013-

1040 08/29/2013; 05/29/2014-08/28/2014; 05/26/2015-09/01/2015

1041 ** Even though one full year of measurements was conducted at the BAO site (12/13/2011-01/09/2013),
1042 only the summer average NH₃ concentration (06/19/2012-08/30/2012) was reported in Fig. 1 to compare with
1043 the NH₃ concentrations at other sites.

1044

Table 2. Summary of summer NH₃ concentrations (units: µg/m³) measured from 2010 to 2015

Site	All years			2010 05/20-09/02			2011 06/2-08/31			2012 06/21-08/29			2013 05/30-08/29			2014 05/29-08/28			2015 05/26-09/01		
	Avg	Max	Min	Avg	Max	Min	Avg	Max	Min	Avg	Max	Min	Avg	Max	Min	Avg	Max	Min	Avg	Max	Min
LE	3.33	5.23	2.27	--	--	--	3.33	5.23	2.27	--	--	--	--	--	--	--	--	--	--	--	--
FC_W	4.09	8.55	1.95	4.13	5.88	3.02	3.76	4.72	2.79	4.63	8.55	2.92	4.45	6.13	1.95	3.78	4.98	2.39	3.83	4.62	2.54
LD	4.40	10.37	2.29	4.17	6.29	2.67	4.81	6.94	3.61	4.57	10.37	2.55	5.08	7.16	2.29	3.68	5.82	2.83	3.99	4.74	2.60
BAO	5.09	7.84	2.85	--	--	--	--	--	--	5.09	7.84	2.85	--	--	--	--	--	--	--	--	--
GC	5.14	7.87	1.81	4.85	7.68	3.01	5.30	7.87	3.87	5.22	7.27	3.74	5.34	7.11	1.81	4.92	6.18	4.07	5.31	7.69	3.33
FC_E	8.56	11.38	5.52	--	--	--	--	--	--	8.36	10.84	5.52	8.30	11.25	5.80	8.99	11.38	6.92	--	--	--
SE	9.10	13.79	4.52	--	--	--	--	--	--	9.34	13.14	6.24	8.52	12.67	4.52	9.70	13.79	7.10	8.66	10.13	6.18
GY	11.34	19.02	5.19	10.39	13.11	7.94	12.90	19.02	8.40	11.07	14.51	6.68	10.52	12.54	5.19	11.72	14.95	9.35	11.63	13.75	7.00
NN	2.66	4.01	0.35	--	--	--	2.78	3.88	1.51	2.59	3.54	1.68	3.01	3.95	1.69	2.84	4.01	1.43	1.60	2.70	0.35
BE	3.07	5.40	1.09	3.18	4.48	1.90	3.33	4.90	2.55	2.99	4.58	2.12	3.00	3.62	1.42	3.15	5.40	2.24	2.43	3.02	1.09
RH	3.27	5.01	1.90	3.27	5.01	1.90	--	--	--	--	--	--	--	--	--	--	--	--	--	--	--
AT	13.75	20.47	6.56	12.55	16.16	9.13	13.78	18.61	8.82	13.70	19.27	9.25	15.13	20.47	6.56	14.49	19.03	10.44	12.08	14.11	6.89
KY	42.73	73.78	23.30	31.05	42.82	23.30	45.96	73.78	30.32	41.65	53.55	25.93	42.67	68.61	25.20	46.57	68.82	29.22	55.14	64.21	47.31
BH	6.17	10.83	3.59	6.54	9.67	3.67	7.26	10.83	5.09	5.45	8.52	3.80	5.99	7.80	3.59	5.62	6.79	4.47	5.07	7.66	4.24